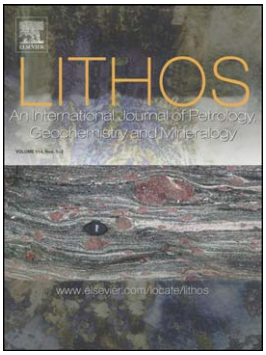

Evaluation of late Permian mafic magmatism in the central Tibetan Plateau as a response to plume-subduction interaction

Bin Liu, Chang-Qian Ma, Pan Guo, Yang Sun, Ke Gao, Yu-Heng Guo

PII: S0024-4937(16)30227-4
DOI: doi: 10.1016/j.lithos.2016.08.011
Reference: LITHOS 4030

To appear in: *LITHOS*

Received date: 21 March 2016
Accepted date: 6 August 2016

Please cite this article as: Liu, Bin, Ma, Chang-Qian, Guo, Pan, Sun, Yang, Gao, Ke, Guo, Yu-Heng, Evaluation of late Permian mafic magmatism in the central Tibetan Plateau as a response to plume-subduction interaction, *LITHOS* (2016), doi: 10.1016/j.lithos.2016.08.011

Evaluation of late Permian mafic magmatism in the central Tibetan Plateau as a response to plume-subduction interaction

Bin Liu[a*], Chang-Qian Ma[b,c]*, Pan Guo[d], Yang Sun[a], Ke Gao[c], Yu-Heng Guo[c]

[a] *School of Geosciences, Yangtze University, Wuhan 430100, China*

[b] *State Key Laboratory of Geological Processes and Mineral Resources, China University of Geosciences, Wuhan 430074, China*

[c] *Faculty of Earth Sciences, China University of Geosciences, Wuhan 430074, China*

[d] *Hubei Geological Survey, Wuhan430000, China*

* Corresponding authors.

E-mail addresses: liubincug@foxmail.com (B. Liu), cqma@cug.edu.cn (C.-Q.Ma)

Telephone: +86 27 69111650

Fax: +86 27 69111650

Abstract

An integrated study of the geochronology, mineralogy, geochemistry and Sr-Nd isotope compositions of the upper Permian Yushu mafic rocks in the central Tibetan Plateau (CTP) was conducted to evaluate the interaction between the Emeishan mantle plume and the Paleo-Tethyan subduction system. These mafic rocks can be geochemically subdivided into three groups. Group 1 rocks yielded a weighted mean $^{206}Pb/^{238}U$ age of 258±2 Ma. They have relatively high TiO_2, FeO_t, Nb/Y and high $\varepsilon_{Nd}(t)$ values and display oceanic island basalts (OIB)-like rare earth and trace element patterns, with obvious enrichment of Nb and Ta. Group 2 and 3 samples yield weighted mean $^{206}Pb/^{238}U$ ages of 258±1 Ma and 257±1 Ma, respectively. Both have relatively low TiO_2, FeO_t, Nb/Y and $\varepsilon_{Nd}(t)$ values and island arc tholeiites (IAT)-like rare earth and trace element patterns with obvious depletion of Nb and Ta. However, the Group 2 rocks have relatively low FeO_t/MgO ratios, but high MgO, $Mg^{\#}$, Cr and Ni contents, resembling primitive magmas. They have lower light rare earth element (LREE), Nb, Ti and Zr contents and higher $\varepsilon_{Nd}(t)$ values than the Group 1 rocks. The geochemical and isotopic variations suggest that the Group 1 rocks might be derived from a plume-related mantle source, whereas Group 2 and Group 3 rocks originated from subduction-modified asthenospheric mantle and lithospheric mantle. Moderate degrees of olivine and clinopyroxene fractionation under low oxygen fugacities (fO_2) appear to be responsible for the Fe-Ti enrichment in the Group 1 rocks. We propose a model involving plume-subduction interaction to explain the geodynamics and generation of the late Permian mafic magmatism in the CTP. The study region was

rifted by the Emeishan mantle plume activity in association with rollback of Longmuco-Shuanghu oceanic lithosphere in late Permian times. Deep melting of the plume source led to the generation of the Group 1 plume-related magmas, whereas shallower melting of the subduction-metasomatized asthenospheric and lithospheric mantle resulted in the generation of the Group 2 and Group 3 subduction-related magmas.

Keywords: Plume-subduction interaction; Mafic; Paleo-Tethys; Yushu; central Tibetan Plateau

1 Introduction

The mantle plume hypothesis was initially proposed to explain particular examples of basaltic volcanisms (e.g., Morgan, 1972) located far from plate boundaries i.e., intraplate volcanism, The most significant types of intraplate volcanism are continental flood basalts, giant oceanic plateaus and aseismic ridges (e.g., Campbell, 2005). Mantle plumes are now defined as rising columns of hot solid materials that probably originate just above the core-mantle boundary and that tend to be located closer to divergent boundaries than to convergent boundaries (e.g., Campbell et al., 2014; Fletcher and Wyman, 2015). However, there are also mantle plumes, such as the Samoa Plume (e.g., Turner and Hawkesworth, 1998), Socorro plume (e.g., Courtillot et al., 2003) and Bowie plume (e.g., Montelli et al., 2006),

located beneath or near slab subduction systems. Such upwelling plumes can interact directly or indirectly with the subduction systems and could result in distinct geodynamic and geochemical deviations from normal subduction system patterns (e.g., Gazel et al., 2011; Whattam and Stern, 2015). Recent computer- and laboratory-based studies have focused on the geodynamic processes of plume-subduction interaction (e.g., Betts et al., 2012; Druken et al., 2014; Gerya et al., 2015; Kincaid et al., 2013). However, detailed empirical studies of basaltic (or mafic) magmatism in response to the interaction between a mantle plume and a subduction system are few.

The Emeishan large igneous province (LIP) is one of the most studied LIPs in the world and covers ~0.3×10^6 km^2 of southwestern China and northern Vietnam (e.g., Shellnutt, 2014). The Emeishan LIP is composed of voluminous flood basalts (low-Ti and high-Ti basalts) and many ore-bearing mafic-ultramafic rocks, as well as alkaline and felsic rocks (e.g., Song et al., 2004; Xiao et al., 2004; Xu et al., 2001). It has been divided into three zones (e.g., He et al., 2003; Fig.1a) and interpreted as having a typical mantle plume origin (e.g., Ali et al., 2005; Chung and Jahn, 1995; He et al., 2007, 2010a; Xu et al., 2004; Zhou et al., 2002). It apparently formed during a short eruption period (<2 Ma) at a time close to the Guadalupian-Loping stratigraphic boundary (~260 Ma) (e.g., Ali et al., 2005; He et al., 2007, 2010a), contemporaneous with a late Capitanian mass extinction (e.g., Shellnutt, 2014; Zhou et al., 2002).

The Emeishan LIP is located near the southeastern margin of the central Tibetan Plateau (CTP; Fig. 1a), a region characterized by the development of a Paleo-Tethyan tectonic-magmatic system (e.g., Metcalfe, 2013; Pan et al., 2012; Yin and Harrison,

2000). Previous studies have shown that some basalts in the CTP were genetically and/or temporally associated with the Emeishan LIP (Fig. 1a; e.g., Song et al., 2004; Xiao et al., 2008; Zi et al., 2010) and raise some interesting questions, including whether the Emeishan mantle plume participated in the generation of Paleo-Tethyan magmas, and if so, how the plume interacted with the Paleo-Tethyan subduction system beneath the CTP.

Upper Permian mafic rocks consisting mainly of gabbros and dolerites are widespread in the Yushu area of the CTP (Fig. 1b). Their formation ages (257-258 Ma) appear be comparable to those of the Emeishan LIP, and they have geochemical compositions similar to those of the Emeishan basalts and/or island arc tholeiits (IAT). These rocks should therefore provide valuable clues about the relationship between the Emeishan mantle plume and the Paleo-Tethys Ocean. In this paper, we provide detailed geochronological, mineralogical, geochemical and isotopic data on these mafic rocks and discuss their petrogenesis and geodynamic settings.

2 Geological backgrounds

The CTP is composed of multiple terranes and suture zones marked by widespread mafic and felsic magmatism (Fig. 1a). It has been divided into tectonic units based on three main boundaries: the Garzê-Litang suture zone, the Jinshajiang suture zone and Longmuco-Shuanghu suture zone (Fig. 1a; e.g., Yang et al., 2012). The tectonic units are represented from north to south locally by the Bayan Har-Songpan Garzê terrane, the Yidun arc terrane and the North Qiangtang terrane

(Fig. 1a).

Along the Jinsha River, the Jinshajiang suture zone (JS) is regarded as an important branch of the eastern Asia Paleo-Tethys Ocean. The Yushu area roughly separates the JS into two different segments, a western segment (WJS) and a southern segment (SJS). Previous studies have focused on the ophiolites, volcanic rocks, granitic intrusions, stratigraphy and palaeontology of the SJS and proposed that the evolution of the SJS included late Devonian-early Carboniferous sea-floor spreading, and Permian-Triassic ocean closure and subsequent continental collision (e.g.,Jian et al., 2009a, 2009b; Metcalfe, 2013; Wang et al., 2000; Zi et al., 2012, 2013). The JS is generally considered to connect with the Ailaoshan suture zone to the southeast (e.g., Wang et al., 2000) and with the Songma suture zone farther to the southeast in Vietnam (e.g., Fan et al., 2010). In contrast, the westward extent of the JS remains hotly debated (e.g., Reid et al., 2005; Yang et al., 2012). The Garzê-Litang suture zone (GLS) separates the Bayan Har-Songpan Garzê terrane from the Yidun arc terrane and the North Qiangtang terrane and has recently been regarded as another important branch of the Paleo-Tethys Ocean (e.g., Liu et al., 2016a; Reid et al., 2005; Yang et al., 2012). Middle to late Triassic magmatic rocks are widespread in the Yidun arc terrane, with the ages ranging from 230 Ma to 201 Ma (e.g., Chen et al., 2014; Wang et al., 2011). The Longmuco-Shuanghu suture zone (LSS) has recently been recognized as the main suture associated with the closure of the Paleo-Tethys Ocean in the Tibetan Plateau (Fan et al., 2015; Hu et al., 2014; Li, 1987; Li et al., 2006, 2007, 2009; Metcalfe, 2013). It contains ophiolitic mélange, eclogite, blueschist

and some ocean island basalt (OIB)-like basalt (Fan et al., 2015; Kapp et al., 2003; Wu et al., 2013). Carboniferous ophiolites (357-345 Ma) have been identified in the LSS by Zhai et al.(2013) and display approximately chemical compositions similar to normal mid-ocean ridge basalt (N-MORB) and enriched mid-ocean ridge basalt (E-MORB). Garnet Lu-Hf isochron ages of 244 Ma and zircon U-Pb ages of 237-230 Ma were interpreted as the time of the peak eclogite-facies metamorphism (e.g., Pullen et al., 2008; Zhai et al., 2011), whereas muscovite ^{49}Ar-^{39}Ar ages of 222-203 Ma were interpreted as the time of retrograde metamorphism or exhumation of the UHP rocks (e.g., Kapp et al., 2003, 2000; Zhai et al., 2009).

The Bayan Har-Songpan Garzê terrane is a huge triangular tectonic unit in the north of the CTP, bounded by the Kunlun-A'nyemaqen suture zone to the north, the JS to the south and the Longmenshan Thrust Belt to the east. It contains the largest volume of Triassic flysch turbidites on Earth (approximately 2.2×10^3 km^3; e.g., Nie et al., 1994) and covers more than 2×10^5 km^2 of the CTP. Triassic sediments were intruded by numerous granitic plutons with ages ranging from 228Ma to 202Ma in its central and eastern regions (e.g., Xiao et al., 2007; Zhang et al., 2007). The Yidun arc terrane is bounded by the SJS to the west and the GLS to the east and is divided into eastern and western parts by the N-S-trending Xiangcheng-Geza Fault. It also has widespread Triassic flysch deposits of the Yidun group, which contains many arc-like Triassic magmatic rocks. The North Qiangtang terrane is bounded by the WJS to the north and the LSS to the south. It consists of upper Palaeozoic meta-sedimentary rocks, Triassic and Jurassic carbonates and terrestrial clastic rocks, and various

igneous rocks. The widespread occurrence of detrital zircons with ages of >500 Ma in the metamorphic rocks suggests the nearby presence of Precambrian crystalline basement (e.g., Kapp et al., 2003).

3 Sample descriptions

The Yushu area is located on the north margin of the North Qiangtang terrane and contains a large volume of Permian to Triassic magmatic rocks (Fig. 1b). We investigated typical upper Permian mafic intrusive rocks, including Yushu gabbros, Haxiu gabbros, Zhiduo dolerites and gabbros from four different locations in the Yushu area (Fig. 1b and Fig. 2). Rock samples were selected from unweathered outcrops for zircon U-Pb age, mineralogical, geochemical and Sr-Nd isotopic composition analysis. Sampling locations are shown in Fig. 1b.

The Yushu gabbros usually occur as dikes intruding low-grade metaclastics. They are primarily composed of clinopyroxene (35-40%), plagioclase (50-60%), hornblende (5%) and some opaque minerals (3-5%) and display a medium-grained texture (Fig. 2a). Clinopyroxene is subhedral and prismatic and is partly replaced by chlorite, epidote and uralite. Most plagioclases are partly altered to sericite, and a few show polysynthetic twinning. The Haxiu gabbros are sheet-like bodies in the clastic rocks and show a medium-grained gabbroic texture (Fig. 2b). These gabbros consist of hornblende (50-55%), clinopyroxene (5-10%), plagioclase (45-55%) and opaque minerals (3-5%). Clinopyroxene is almost entirely replaced by hornblende, chlorite and uralite, except for a few remnants of clinopyroxene in the hornblende. The Zhiduo

dolerites and gabbros occur as rock slices and/or masses in the Duocai mélange. They exhibit a fine- to medium-grained ophitic texture and contain clinopyroxene (5-10%), hornblende (35-40%), plagioclase (50-50%), biotite (5%) and accessory opaque minerals (3-5%) (Fig. 2c). Most of the gabbros are medium-grained and are composed of clinopyroxene (5-10%), hornblende (30-40%) and plagioclase (50-60%) (Fig. 2d). Accessory minerals include garnet, epidote and opaque minerals.

4 Analytical methods

Zircon grains were separated for U-Pb isotopic analyses by mechanical crushing, conventional heavy liquid and magnetic techniques and hand picking under a binocular microscope. Representative grains were mounted in epoxy resin and polished. Transmitted and reflected light photomicrographs and cathodoluminescence (CL) images of the chosen grains were obtained to select appropriate analytical sites. Zircon U-Pb isotopic analyses were conducted using a laser ablation inductively coupled plasma-mass spectrometer (LA-ICP-MS) at the State Key Laboratory of Geological Processes and Mineral Resources (GPMR), China University of Geosciences (Wuhan). A GeoLas 2005 was used to perform the laser sampling, and an Agilent 7500a ICP-MS instrument was used to acquire ion-signal intensities. Detailed operating conditions for the laser ablation system and ICP-MS instrument and details on the data reduction are given by Liu et al. (2008a; 2010a, 2010b). The common lead correction was applied using the method of Andersen (2002), while the Concordia age plots and weighted mean ages were obtained using ISOPLOT software (Ludwing,

2003).

Major element abundances were determined using a Regaku3080E1-type XRF spectrometer at the Analytical Institute of the Bureau of Geology and Mineral Resources (BGMRHP), Hubei Province, China, with an analytical precision better than 5%. Rare earth and trace elements were measured using an Agilent 7500a ICP-MS at the State Key Laboratory of Geological Processes and Mineral Resources (GPMR), China University of Geosciences (Wuhan). Samples were digested by HF + HNO_3 in Teflon bombs before testing. The detailed sample digestion procedure for the ICP-MS analyses and the analytical precision and accuracy for trace elements are described by Liu et al. (2008b).

Whole-rock Sr and Nd isotopic ratios were determined on a Finnigan Triton thermo-ion mass isotope spectrometer at GPMR, China University of Geosciences (Wuhan). Details on the experimental procedures and analytical precision were described in Gao et al. (2004). The reported $^{87}Sr/^{86}Sr$ and $^{143}Nd/^{144}Nd$ ratios were normalized to $^{88}Sr/^{86}Sr=8.375209$ and $^{146}Nd/^{144}Nd=0.721900$, respectively. The average $^{143}Nd/^{144}Nd$ ratios of the JNdi-1 standard measured during the sample runs was 0.512118±9 (2σ) and the NBS987 standard gave $^{87}Sr/^{86}Sr$ as 0.710274±9 (2σ).

Clinopyroxene compositions were obtained by using a JEOL-JXA-8100 electron microprobe at the GPMR. The analytical conditions and procedures have been described by Zheng et al. (2009). Most of the illustrations in this paper were produced using GEOKIT software (Lu, 2004).

5 Results

5.1 Zircon U-Pb ages

Four representative zircon samples were selected for LA-ICP-MS zircon U-Pb isotopic analyses. The results are listed in Supplementary Table S1, and CL images and analytical sites of representative zircons are shown in Fig. 3.

The Yushu gabbroic sample (RN06-1) was collected from the location of N 33°09.209' and E 96°56.731′ and is a representative of the Group 1 rocks as defined in the following section. All the zircons are transparent, colourless or slightly yellow, with grain sizes ranging from 50 μm to 150 μm. Most have subhedral or euhedral columnar crystals and display obvious broad-spaced oscillatory zoning in the CL images (Fig. 3a). All twenty-three analyses conducted on sample RN06-1 returned high Th/U ratios in the range of 0.84 to 1.34 and yielded a coherent age group with a weighted mean $^{206}Pb/^{238}U$ age of 258±2 Ma (MSWD=2.5, Fig. 3b), which we interpret as the crystallization age of the Yushu mafic rocks. Within analytical error, this age is the same as previously published SHRIMP zircon U-Pb isotopic analyses of nearby Rangnianggongba mafic rocks (258.4±2.9 Ma; Yong et al., 2011), confirming the accuracy of the LA-ICP-MS analyses in this study.

The Zhiduo doleritic sample (NQ05-1), a representative of the Group 1 rocks was collected from the site at N 33°47.427′ and E 95°28.933′. The zircons are colourless and subhedral, columnar or tabular, with grain sizes of 50-120 μm. All have broadly spaced oscillatory zoning (Fig. 3a) and high Th/U ratios (0.68-2.51). Eighteen analyses yielded a weighted mean $^{206}Pb/^{238}U$ age of 258±2 Ma (MSWD=1.02; Fig.

3b), which we interpret as the crystallization age of the Zhiduo dolerites.

The Haxiu gabbroic sample (HX01-1), a representative of the Group 2 rocks (see the next section for details), was collected from the site at N 33°21.060′ and E 96°27.849′. All the zircons are transparent and colourless, with grain sizes of 30-130 μm. Most have subhedral tabular or columnar crystals and high Th/U ratios (0.87-11.61) and show typical broadly spaced oscillatory zoning in the CL images (Fig. 3a), suggesting a magmatic origin. Twenty-one analyses were performed, and they yielded a weighted mean $^{206}Pb/^{238}U$ age of 258±1 Ma (MSWD=1.9; Fig. 3b), which was taken to be the crystallization ages of the Haxiu hornblende gabbros. Although other zircons also have subhedral columnar crystals and high Th/U ratios (0.93-1.41) and some of them show broadly spaced oscillatory zoning, five analyses yielded relatively old $^{206}Pb/^{238}U$ ages including 387 Ma, 406 Ma, 422 Ma, 908 Ma and 2139 Ma (Fig. 4b). We interpret these older grains as inherited zircons.

The Zhiduo gabbroic sample (PNQ29-2) was collected from the location of N33°47.234′ and E95°28.695′ and is the representative of the Group 3 rocks as defined in the following section. The zircons are transparent, colourless or light green, subhedral or euhedral columnar crystals, with grain sizes of 50-130 μm, broadly spaced oscillatory zoning in the CL images (Fig. 3a) and high Th/U ratios (0.87-1.65). Twenty-one analyses performed on the zircons yielded a weighted mean $^{206}Pb/^{238}U$ age of 257±1 Ma (MSWD=1.06; Fig. 3b), which we consider to be the crystallization age of the Zhiduo gabbros.

5.2 Whole-rock geochemistry

Major, rare earth and trace element analyses of the selected samples are listed in Table 1. Most samples have relatively low CO_2+H_2O^+ values (Table 1). The mafic samples are geochemically subdivided into Groups 1, 2 and 3 based on Nb/Y ratios, FeO_t and TiO_2 contents, and incompatible element patterns.

Group 1 samples, from the Yushu gabbros and Zhiduo dolerites, have variable MgO and $Mg^{\#}$ values ($Mg^{\#}=Mg^{2+}/(Mg^{2+}+Fe_t^{2+})$), and relatively high TiO_2 (mostly >2.5 wt.%)， FeO_t and Nb/Y values (Table 1). All the samples plot in the alkaline basalt field on a Nb/Y vs. Zr/TiO_2 diagram (Fig. 4a). Most samples show strong Fe and Ti enrichment on the ($CaO+Al_2O_3$)-(FeO_t+TiO_2)-MgO diagram in comparison with normal gabbros, similar to mafic rocks from Panzhihua in China, East Greenland and northern Somalia (Fig. 4b; e.g., Aden and Frizzo, 1996; Brooks et al., 1991; Zhou et al., 2005). Chondrite-normalized rare earth elements (REE) patterns uniformly display enrichment of light REEs (LREEs) relative to heavy REEs (HREEs), with $(La/Yb)_N$ ratios of 5.60-7.34 (Fig. 5a). All the samples show slight negative or positive Eu anomalies (Eu/Eu*=0.89-1.14). On an N-MORB-normalized trace element spider diagram, most samples are characterized by enrichment of large ion lithophile elements (LILEs, e.g., Th, U, LREE) and high field strength elements (HFSEs, e.g., Nb, Ta, Ti), comparable to OIBs and the Emeishan high-Ti basalts and mafic intrusions (Fig. 5b).

Group 2 samples, represented by the Haxiu hornblende gabbros, show relatively low TiO_2, FeO_t and Nb/Y values (Table 1), and belong to the sub-alkaline basalt

series (Fig. 4a). On the $(CaO+Al_2O_3)$-(FeO_t+TiO_2)-MgO diagram, most samples plot along a straight line between plagioclase and clinopyroxene, similar to normal gabbros (Fig. 4b). All the samples have relatively low FeO_t/MgO ratios (0.57-0.83), but high values of MgO (10.19-16.54 wt.%), $Mg^{\#}$ (68-76), Cr (684-895 ppm) and Ni (138-486 ppm), resembling primitive magmas (Tatsumi and Eggins, 1995). They exhibit weak LREE enrichment ($(La/Yb)_N$=1.01-1.24) and slight negative or positive Eu anomalies (Eu/Eu*= 0.88-1.05) on the chondrite-normalized REE diagram (Fig. 5c). On the N-MORB-normalized trace element spider diagram, the samples show moderate enrichment of LILEs (e.g., Th, U and LREEs) and obvious depletion of HFSEs (e.g., Nb, Ta, Ti), similar to subduction-related basaltic rocks (e.g., Island arc tholeiites (IATs)).

Group 3 samples from the Zhiduo gabbros have relatively high SiO_2, moderate TiO_2 and FeO_t contents, variable MgO and $Mg^{\#}$ values and low Nb/Y ratios compared with the other two groups (Table 1). On the Nb/Y vs. Zr/TiO_2 diagram, all the samples plot in the sub-alkaline basalt field (Fig. 4a). The $(CaO+Al_2O_3)$-(FeO_t+TiO_2)-MgO diagram shows slight Fe and Ti enrichment in comparison with the normal gabbros (Fig. 4b). Their chondrite-normalized REE patterns display strong enrichment of LREEs relative to HREEs ($(La/Yb)_N$ =1.56-4.74), with weak negative Eu anomalies (0.81-0.92) (Fig. 5e). On the N-MORB-normalized trace element spider diagram, the samples are characterized by strong enrichment of LILEs (e.g., Th, U and LREEs) and weak depletion of HFSEs (e.g., Nb, Ta and Ti) and are generally comparable to subduction-related basaltic rocks (e.g., IATs; Fig. 5f).

5.3 Sr-Nd isotope compositions

The Sr-Nd isotope composition data are given in Table 2, and the initial ratios are calculated back to a timing of 260 Ma. Group 1 rocks have relatively high $\varepsilon_{Nd}(t)$ values and low initial Sr ratios (Table 2). On an $\varepsilon_{Nd}(t)$ vs. I_{sr} diagram, all Group 1 samples plot in the Emeishan high-Ti basalt field and most of them have $\varepsilon_{Nd}(t)$ values similar to the Funing high-Ti mafic intrusions in the Emeishan LIP (Zhou et al., 2006; Fig. 6a). The Group 2 rocks have moderate I_{sr} and $\varepsilon_{Nd}(t)$ values (Table 2). Group 3 samples are characterized by relatively low $\varepsilon_{Nd}(t)$ values and high I_{sr} (Table 2). The samples of all three groups retain constant $\varepsilon_{Nd}(t)$ values with decreasing $Mg^{\#}$ (Fig. 6b), suggesting insignificant crustal assimilation.

5.4 Clinopyroxene chemistry

The content of major element analyses and calculated parameters of clinopyroxenes from the Group 1 samples are given in Supplementary Table S2 and plotted in Fig. 7. The pyroxenes are characterized by relatively high MgO, TiO_2 and FeO_t contents and low Al_2O_3 and Cr_2O_3 contents (Table S2), similar to pyroxenes from the Panzhihua mafic-ultramafic rocks of the Emeishan LIP (Fig. 7; Pang et al., 2009). All the pyroxenes are assigned to the Ca-Fe-Mg pyroxene group under the Morimoto (1988) classification, and the Wo-En-Fs classification diagram identifies the pyroxenes as augites (Fig. 7a). On the diagram of Al_z (in percent of total tetrahedral cations) vs. TiO_2, they exhibit a rift-cumulate trend (Fig. 7b; Loucks,

1990).

6 Discussion

6.1 Fractional crystallization and crustal assimilation

It is necessary to consider the effects of fractional crystallization and crustal assimilation on magma compositions before evaluating potential mantle sources for the three group rocks.

Group 1 and Group 3 rocks have relatively low and variable $Mg^{\#}$, Cr and Ni values (Table 1), suggesting that they may have experienced some degree of fractional crystallization from mantle-generated parental magmas. Positive correlations among the Cr, Ni, Sc/Y and $Mg^{\#}$ values and constant CaO/Al_2O_3 ratios with decreasing $Mg^{\#}$ (Fig. 8) suggest fractional crystallization of olivine, clinopyroxene and plagioclase (e.g., Naumann and Geist, 1999). Apatite and Fe-Ti oxide fractionation probably did not play an important role in the generation of these two groups of rocks, as indicated by negative or nil correlations between P_2O_5, TiO_2, FeO_t and $Mg^{\#}$ (Fig. 8). Group 2 rocks have high MgO, $Mg^{\#}$, Cr and Ni contents (Table 1), comparable to those of primitive magmas (e.g.,Tatsumi and Eggins, 1995). However, fractionation of olivine and some clinopyroxene cannot be completely discounted because of positive correlations among the Cr, Ni, Sc/Y and $Mg^{\#}$ values (Fig.8). The straight line between the plagioclase and clinopyroxene compositions on the $(CaO+Al_2O_3)$-(FeO_t+TiO_2)-MgO diagram displayed by the Group 2 gabbros (Fig. 4b) could indicate fractionation of these two minerals. All three groups of rocks could have experienced different

types of differentiation of olivine, clinopyroxene and plagioclase.

Crustal contamination accompanied by fractional crystallization (AFC) often plays an important role in mafic magma evolution and can modify the chemical and isotopic compositions of the initial magmas (e.g., Halama et al., 2004). Crustal contamination decreases TiO_2 and P_2O_5 contents, but increases LILE, K_2O and Na_2O contents (e.g., Zhao and Zhou, 2007). Group 1 and Group3 rocks exhibit increasing TiO_2 and P_2O_5 contents with decreasing $Mg^{\#}$ values (Fig. 8), which is inconsistent with crustal contamination. The rocks in these two groups display no correlation between Nb/La and $Mg^{\#}$ and exhibit constant $\varepsilon_{Nd}(t)$ values with decreasing $Mg^{\#}$. These patterns are not typically associated with crustal contamination (Fig. 6b and 8). Although there are older inherited zircons in the Group 2 rocks (Fig. 3), crustal contamination appears to be negligible because of the negative correlation between TiO_2 and $Mg^{\#}$; the constant P_2O_5, Nb/La and $\varepsilon_{Nd}(t)$ values with decreasing $Mg^{\#}$; and the Nb/La and Nb/Ce ratios that are lower than those of the primitive mantle, average bulk crust and average lower crust (Taylor and McLennan, 1985).

6.2 Mantle sources and magma generation

Group 1 rocks have relatively high Nb/Y ratios (Table 2) and belong to the alkaline basalt series (Fig. 4a). As described above, most samples display evidence of insignificant crustal contamination and have OIB-like REE and trace element patterns, with obvious enrichment of Nb and Ta (Fig. 5). Experiments on Fe-Ti oxide/melt partition coefficients have shown that HFSEs (e.g., Nb, Ta, Zr and Hf) are usually

moderately compatible in oxides (e.g., Klemme et al., 2006; Nielsen and Beard, 2000) and that the presence of excess Fe-Ti oxides can result in elevated ratios of Nb and Ta relative to other trace elements (e.g., REE, U and Th). The low or negative correlations among FeO_t, TiO_2 and $Mg^{\#}$ suggest an insignificant contribution of fractionation or accumulation of Fe-Ti oxides in the magmas (Fig. 8). The constant Nb/La ratios with increasing TiO_2 content further preclude the presence of excess Fe-Ti oxides (Fig. 9a). The enrichment in Nb and Ta appears to be a feature of the primitive magma.

The generation of mafic rocks with an OIB-like geochemical composition has generally been attributed to mantle plume activity or mantle heterogeneity (e.g., Hanan et al., 2000; Saccani et al., 2013; Weaver, 1991). Some lines of evidence support a mantle plume hypothesis for the Yushu rocks. The Nb/Y vs. Zr/Y diagram has been shown to be effective at distinguishing between mafic melts derived from plume sources and those derived from non-plume sources because the Nb/Y and Zr/Y ratios are insensitive to the influence of the degree of mantle melting, source depletion, crustal contamination and subsequent alteration (Fitton et al., 1997). On the Nb/Y vs. Zr/Y diagram (Fig. 9b), all the samples plot in or near the OIB and oceanic plateau basalt fields, indicating a plume-related source. Previous studies of the Emeishan LIP suggest that the high-Ti basalts were generated by deep melting in a plume head, whereas the low-Ti basalts were generated by shallow melting in a plume head with significant lithospheric inputs (e.g., Chung and Jahn, 1995; He et al., 2010b; Xiao et al., 2004; Xu et al., 2001). The Group 1 rocks have relatively high TiO_2 contents

(mostly >2.5 wt.%), analogous to the Emeishan high-Ti basalts and Funing high-Ti mafic intrusions of the Emeishan LIP (TiO_2=1.55-4.44 wt.%; Zhou et al., 2006). Most of Group 1 rocks display similar REE and trace element patterns to Emeishan high-Ti basalts and the Funing high-Ti mafic intrusions (Fig. 5a, b). All the Group 1 rocks have relatively high $\varepsilon_{Nd}(t)$ values and low initial Sr ratios (Table 2) and plot in the field of the Emeishan high-Ti basalts in the $\varepsilon_{Nd}(t)$ vs. I_{sr} diagram (Fig. 6a). Although initial Sr ratios are relatively dispersed, their $\varepsilon_{Nd}(t)$ values are comparable to those of the Funing high-Ti mafic intrusions and OIBs (Fig. 6a). The Nb/Yb vs. Zr/TiO_2, Th/Yb vs. Nb/Yb and Nb/Y vs. Zr/Y diagrams show significant overlaps between the Group 1 rocks and Emeishan high-Ti basalts (Figs. 4a, 9b, 10a). Additionally, clinopyroxenes from the Group 1 rocks are mainly characterized by relatively high MgO, TiO_2 and FeO_t contents, low Al_2O_3 and Cr_2O_3 contents (Table 3) and a rift-cumulate trend (Fig. 7b), similar to pyroxenes from the Panzhihua mafic-ultramafic rocks related to the Emeishan mantle plume. Based on these results, we suggest that the Group 1 rocks might have originated from a plume-related mantle source.

Unlike Group 1, all samples from Groups 2 and Group 3 are characterized by LREE and LILE enrichment and strong HFSE depletion (e.g., Nb, Ta and Ti) relative to N-MORB (Fig. 5), similar to subduction-related basaltic magmas (e.g., IATs). They have relatively low $\varepsilon_{Nd}(t)$ values and high I_{sr} values (Table 2), suggesting a more enriched mantle. On the Th/Yb vs. Nb/Yb diagram, both groups of rocks plot above the MORB-OIB array, indicating involvement of crustal components in their

generation (Fig. 10a). Crustal contamination and source mixing are generally considered as the two main mechanisms for incorporating crustal components into mafic rocks (e.g., Dai et al., 2015; Zhao et al., 2013). As discussed above, crustal contamination did not play a major role during the generation of the two groups of rocks; therefore, their arc-like compositions should be attributed to source mixing between mantle and crustal components via delamination or slab subduction (e.g., Wang et al., 2013). However, there is no regional geological evidence for delamination in late Permian times. Thus, the high La/Nb,and Zr/Nb and low Nb/U ratios further suggest that the two groups of samples were derived from a mantle source metasomatized by subduction-derived components (Fig. 10b). The Group 2 rocks have lower LREE/HREE and Nb/Yb ratios and higher $\varepsilon_{Nd}(t)$ values than the Group 3 rocks, suggesting that they were not derived from the same mantle sources. The compositions of the Group 2 rocks are similar to those of the lavas of the intraoceanic South Sandwich arc (Fig. 10a) which are considered to be derived from sub-arc asthenosphere because no continental lithosphere exists beneath the arc (e.g., Pearce et al., 1995). In addition, Leat et al. (2002) had identified two different types of primitive mafic melts in the Antarctic Peninsula, a typical continental arc, and suggested that they were derived from subduction-modified sub-arc asthenospheric and lithospheric mantle, respectively. The asthenosphere-derived group of mafic melts are usually more depleted in HFSEs (e.g., Ti, Zr and Nb) and LREEs than the lithosphere-derived group. All the Group 2 rocks have high MgO, $Mg^{\#}$, Cr and Ni contents (Table 1), similar to those of primitive magmas (e.g., Tatsumi and Eggins,

1995). Additionally, they also show relatively low LREEs, Nb, Ti and Zr, comparable to the asthenosphere-derived group of primitive mafic melts as described by Leat et al.(2002)(Figs. 5c,d and 10a). Therefore, we interpret the Group 2 rocks to be partial melts of subduction-modified asthenospheric mantle. In constrast, the Group 3 rocks have relatively high LREE, Nb, Ti and Zr contents, comparable to the lithosphere-derived group of primitive mafic melts (Figs. 5e, f and 10a), suggesting that they might be generated by partial melting of subduction-modified lithospheric mantle.

The first-row transition elements (e.g., Zn/Fe_t values) can offer a useful approach for fingerprinting lithological features of the sources of mafic rocks emplaced in the continental crust (e.g., Dai et al., 2012; Le Roux et al., 2011, 2010; Murray et al., 2015). Experimental results have proved that there is minimal fractionation of Zn, Fe and Mn if the mantle lithology is peridotite. Zn/Fe_t ratios can be modified by clinopyroxene or garnet fractionation during mantle melting rather than by fractional crystallization of olivine, and the Zn/Fe_t ratios of peridotite–derived melts ($Zn/Fe_t \times 10^4 = 9 \pm 1$) are typically lower than those of pyroxenite-derived melts ($Zn/Fe_t \times 10^4 = 13\text{-}20$). The Group 2 rocks have relatively high MgO, $Mg^{\#}$, Cr and Ni contents, similar to primitive magmas, and have experienced minimal fractionation of clinopyroxene and olivine. They have low Zn/Fe_t ratios of 8.14-10.18 and overlap with the field of typical peridotite and MORB (Fig. 11a), suggesting they might have originated from peridotite. Although some evidence suggests that the Group 1 rocks have undergone some degree of clinopyroxene fractionation, their Zn/Fe_t ratios, which

are lower than typical pyroxenite-derived melts, indicate their mantle lithology was more likely peridotite rather than pyroxenite (Fig. 11a). It is difficult to verify the mantle lithology of Group 3 because most of the Group 3 rocks have experienced higher degrees of clinopyroxene fractionation and display relatively high and scattered Zn/Fe_t ratios relative to the peridotite-derived melts (Fig. 11a). However, one Group 3 sample (DC50-1) with a high $Mg^{\#}$ (60) and low Zn/Fe_t ratio (9.49) suggests that the Group 3 rocks might be derived from a peridotite mantle source (Fig. 11a). REE ratios, such as Dy/Yb, Sm/Yb and La/Yb, are widely used to determine the mantle source and the degree and depth of mantle melting (e.g., Aldanmaz et al., 2000; McKenzie and O'Nions, 1991; Volkert et al., 2015). Mafic melts derived from a spinel-bearing mantle would have lower Dy/Yb and Sm/Yb ratios than melts generated by a garnet-bearing mantle. All the Group 1 rocks have relatively high Dy/Yb and Sm/Yb ratios and plot below the garnet+spinel peridotite melting curve and above the spinel peridotite melting curve (Fig. 11b), indicating a spinel+minor garnet-bearing peridotite mantle. In contrast, the Group 2 and Group3 rocks have low Dy/Yb and Sm/Yb ratios, suggesting they might have formed in the spinel stability field (Fig. 11b).

6.3 Mechanism of Fe-Ti enrichment in the Group 1 mafic rocks

Although we have proposed partial melting of a plume-related spinel+minor garnet-bearing peridotite mantle as the mechanism responsible for the geochemical and Sr-Nd isotopic variations in the Group 1 mafic rocks, the cause of the strong Fe

and Ti enrichment in comparison with normal gabbros remains unclear. Several models have been proposed to explain Fe-Ti enrichment in mafic rocks in many studies, but there is no consensus (e.g., Peng et al., 2013). Proposed mechanisms include (1) partial melting of a peridotite source containing lenses of Fe-rich eclogite (Gibson, 2002); (2) liquid immiscibility (Zhou et al., 2005); (3) derivation from a Fe-Ti rich mantle (Wang et al., 2008); and (4) varying degrees of olivine and clinopyroxene fractionation under low oxygen fugacities (fO_2) (Clague and Bunch, 1976; Peng et al., 2013; Perfit et al., 1983).

Although partial melting of a peridotite source containing Fe-rich eclogite lenses at <3.0 GPa could generate high-Fe melts with OIB- or MORB-like compositions and high Al_2O_3 (>15 wt.%), $\varepsilon_{Nd}(t)$ (up to +6) and $(Nb/La)_{PM}$ (>1) values (Gibson, 2002; Herzberg and Zhang, 1996), this is not the case for the Fe-Ti-rich rocks in this paper because all the Group 1 rocks have lower Al_2O_3 (12.26-16.19 wt.%), $\varepsilon_{Nd}(t)$ (0.02-0.7) and $(Nb/La)_{PM}$ (0.70-1.01) values. Liquid immiscibility has recently been proposed to explain Fe-Ti enrichment in layered intrusions worldwide, such as the Skaergaard intrusion in Greenland (e.g., Jakobsen et al., 2011) and the Panzhihua intrusion in the Emeishan LIP in China (e.g., Zhou et al., 2005). However, the rock associations and field outcrops of the Group 1 rocks differ from those of the mentioned layered intrusions, which contain low-Si and high-Fe-Ti mafic rocks and have coeval high-Si felsic rocks. It is a possible that the Fe-Ti enrichment was a primary feature of the parent magmas derived from the mantle source (e.g., Wang et al., 2008), but the migration of such a high-Fe-Ti magmas would be difficult due to its unusually high

density. Another way to generate Fe-Ti-rich melts is for the source to undergo varying degrees of olivine and clinopyroxene fractionation under low oxygen fugacities (fO_2) (e.g., Clague and Bunch, 1976; Perfit et al., 1983). Experiments and geological observations have shown that high degrees (e.g., 65-73%) of olivine and clinopyroxene fractionation can generate Fe-Ti-rich melts and that low fO_2 delays saturation of Ti-magnetite and promotes Fe-Ti enrichment in residual magmas (e.g., Li et al., 2014; Peng et al., 2013). All the Group 1 rocks have relatively low and variable $Mg^{\#}$, Cr and Ni values (Table 3) and exhibit positive correlations among Cr, Ni, Sc/Y and $Mg^{\#}$ (Fig. 8), supporting models that invoke fractional crystallization of olivine and clinopyroxene (e.g., Naumann and Geist, 1999). Negative or nil correlations among TiO_2, FeO_t and $Mg^{\#}$ further suggest crystallization of Fe-Ti oxides during a late stage of magma evolution, which is also supported by microscopic petrography. Thus, we conclude a moderate degree of olivine and clinopyroxene fractionation under low oxygen fugacities (fO_2) is the most likely interpretation for the Fe-Ti enrichment in the Group 1 rocks.

6.4 Plume-subduction interaction

As described above, the rocks of both Group 2 and Group 3 display REE and trace element patterns similar to those of subduction-related rocks, such as IATs (Fig. 5c-f). Additionally, the geochemical and isotopic compositions of Group 2 and 3 suggest derivation from subduction-modified asthenospheric and lithospheric mantle, respectively. Therefore, there is a close genetic relationship between these rocks and

slab subduction.

We propose two main hypotheses involving late Permian slab subduction in the study area, incorporating S-directed subduction of the Jinshajiang Ocean and N-directed subduction of the Longmuco-Shuanghu Ocean (e.g., Xu et al., 2013; Yang et al., 2011, 2014). The Jinshajiang Paleo-Tethys Ocean is represented by the JS, which can be divided into the WJS and the SJS in the Yushu area. Previous studies have proposed that the evolution of the SJS involved late Devonian to early Carboniferous sea-floor spreading, Permian to Triassic ocean closure, and subsequent continental collision (e.g., Jian et al., 2009a, 2009b; Metcalfe, 2013; Zi et al., 2013, 2012), but there is no agreement about whether the WJS underwent the same tectonic evolution as the SJS. Recent geochronological studies on the ophiolites in the WJS yield ages of 240-232 Ma (e.g., Duan et al., 2009; Zhang et al., 2012), significantly later than those of the E-MORB-type ophiolites in the SJS (346-341 Ma; Jian et al., 2009b) but similar to those of the Triassic ophiolites in the GLS (236-234Ma; Liu et al., 2016a). Detailed studies have revealed that the deformational history and stratigraphy of the Yushu area are continuous with the Yidun arc terrane (e.g., Reid et al., 2005; Yang et al., 2012). Coeval Triassic arc magmatism on the northern margin of the North Qiangtang terrane and Yidun arc terrane features the same peak age of ~215 Ma (e.g., Liu et al., 2016b; Reid et al., 2005; Yang et al., 2012), indicating that the WJS experienced a tectonic evolution similar to the GLS rather than the SJS. The Longmuco-Shuanghu Ocean is being increasingly accepted as the main Paleo-Tethys Ocean in the Tibetan Plateau (e.g., Metcalfe, 2013; Zhai et al., 2013). Zhai et al. (2013)

identified N-MORB/E-MORB-like ophiolites with U-Pb ages of 357-345 Ma in the LSS, suggesting that a Paleo-Tethys ocean basin existed in Carboniferous times. A suite of upper Permian to Lower Triassic volcanic rocks with U-Pb ages of 275-248 Ma has been identified in the North Qiangtang Terrane, supporting northward subduction of the Longmuco-Shuanghu oceanic plate (e.g., Yang et al., 2011). In view of the crystallization ages and spatial distribution of the Group 2 and Group 3 rocks, we suggest that the generation of these rocks was related to N-directed subduction of the Longmuco-Shuanghu Ocean.

The Emeishan LIP covers ~0.3×10^6 km^2 of southwestern China and northern Vietnam (e.g., Shellnutt, 2014) near the southeastern margin of the central Tibetan Plateau which is characterized by the development of the Paleo-Tethyan tectonic-magmatic system (e.g., Metcalfe, 2013; Xu et al., 2013; Yin and Harrison, 2000). However, whether the Emeishan mantle plume participated in the Paleo-Tethyan evolution is unresolved. Previous studies showing that some basalts in the CTP were to some extent genetically and/or temporally associated with the Emeishan LIP (e.g., Song et al., 2004; Xiao et al., 2008; Zi et al., 2010) support the involvement of the Emeishan mantle plume in the Paleo-Tethyan evolution of the CTP. For example, Zi et al. (2010) reported on the Dashibao high-Ti basalts in the Songpan Garzê terrane and suggested that these basalts were integral parts of the Emeishan LIP. Xiao et al. (2008) reported that high-Ti basalts in the SJS have similar geochemical compositions to Emeishan flood basalts and proposed that the beginning of Jinshajiang Paleo-Tethyan evolution was caused by the Emeishan mantle plume.

The crystallization age of the Group 1 rocks of 258±2 Ma is identical within error to the eruption age of the Emeishan flood basalts (~260 Ma; e.g., Ali et al., 2005; He et al., 2007, 2010). Clinopyroxenes from the Group 1 rocks exhibit an obvious rift-cumulate trend, which is inconsistent with clinopyroxenes from subduction-related mafic rocks associated with back-arc or arc settings but is similar to the pyroxenes from the Panzhihua mafic-ultramafic rocks of Emeishan LIP (Fig.7). Most of the Group 1 rocks have high TiO_2 contents (>2.5 wt.%) and OIB-like trace element patterns, comparable to the Emeishan high-Ti basalts. The geochemical and isotopic variations suggest that they were derived from a plume-related mantle source, similar to the sources of the Emeishan high-Ti basalts and mafic intrusions (e.g., He et al., 2010b; Xiao et al., 2004; Zhou et al., 2006). These conclusions strongly indicate that there is a genetic relationship between the Group 1 rocks and the Emeishan mantle plume.

Correlations of the late Mesoproterozoic to Palaeozoic strata and their flora and fauna among the Songpan-Garzê and Yidun arc terranes and the South China Block indicate that these regions were contiguous until the late Permian (e.g., Chang, 2000; Peng et al., 2014; Song et al., 2004; Weislogel, 2008; Yin and Harrison, 2000). Recent studies have also revealed that the North Qiangtang terrane has Cathaysian affinity (Ding et al., 2011) and that it developed Permian flora and fauna comparable to the South China Block (Metcalfe, 2013). Geochronological studies on the ophiolites in the WJS and GLS have produced ages of 240-232Ma (e.g., Duan et al., 2009; Liu et al., 2016a; Zhang et al., 2012), and the generation of ophiolites is considered to be

related to back-arc basin spreading in response to the rollback of the Longmuco-Shuanghu oceanic lithosphere (Liu et al., 2016a). SHRIMP and LA-ICP-MS zircon U-Pb data have demonstrated that the subduction-related magmatism in the North Qiangtang terrane started as early as 275 Ma and lasted until 248 Ma (Yang et al., 2011). The Group 2 and Group 3 mafic rocks in this study yielded $^{206}Pb/^{238}U$ ages of 258-257 Ma, suggesting that the rollback of the Longmuco-Shuanghu oceanic lithosphere have began in the late Permian. Based on the above considerations, we suggest that the Garzê-Litang Paleo-Tethys Ocean could not have been a large-scale ocean until the late Permian and that the North Qiangtang terrane was not very far from the Songpan Garzê terrane and South China Block at that time. Therefore, the identification of basaltic rocks that are temporally and genetically associated with the Emeishan basalts in the Songpan Garzê (Li et al., 2016; Zi et al., 2010), Yidun arc (Song et al., 2004) and North Qiantang (this study) terranes suggests that the Emeishan mantle plume may have participated in the initial rifting and development of the back-arc basin at the triple junction of the CTP (Fig. 1a).

Therefore, we propose a scenario that explains the geodynamics and generation of the late Permian mafic rocks in the CTP (Fig. 12). The sub-continental lithospheric and asthenospheric mantle was modified by subduction-derived components when the Longmuco-Shuanghu oceanic lithosphere was subducted under the North Qiangtang terrane. The study region was rifted by the Emeishan mantle plume activity in combination with rollback of the Longmuco-Shuanghu oceanic lithosphere in response to its increasing density in late Permian times. Deep melting of the plume

source led to the generation of the Group 1 plume-related magmas, whereas shallower melting of the subduction-metasomatized asthenospheric and lithospheric mantle resulted in the generation of the Group 2 and 3 subduction-related magmas.

7 Conclusions

(1) Three groups of samples yield weighted mean $^{206}Pb/^{238}U$ ages of 258±2 Ma, 258±1 Ma and 257±1 Ma, which are identical within error to the eruption ages of the Emeishan flood basalts (~260 Ma).

(2) The geochemical and isotopic variations indicate that the Group 1 rocks were derived from a plume-related mantle source and that the Group 2 and Group 3 rocks originated from subduction-modified asthenospheric mantle and subduction-modified lithospheric mantle, respectively.

(3) A model involving plume-subduction interaction accounts for the geochemical variations in the late Permian mafic rocks in the Yushu area.

Acknowledgements

This work was financially supported by the National Nature Science Foundation of China (Grant 41502050 & 41272079), China Geological Survey (No.DD20160022 & 12120115026901) and the Yangtze Youth Fund (2015cqn29). We thank Yusheng Liu, Zhaochu Hu, Haihong Chen, Shu Zheng and Lian Zhou for their help with analytical work. We thank Professor Roger Mason for his meticulous language editing and constructive reviews of this article. We also thank two anonymous reviewers for

their valuable comments and constructive suggestions.

References

Aden, A., Frizzo, P., 1996. Geochemistry and origin of low and high TiO_2 mafic rocks in the Barkasan complex: a comparison with common Neoproterozoic gabbros of northern Somali crystalline basement. Journal of African Earth Sciences 22, 43-54.

Aldanmaz, E., Pearce, J.A., Thirlwall, M.F., Mitchell, J.G., 2000. Petrogenetic evolution of late Cenozoic, post-collision volcanism in western Anatolia, Turkey. Journal of Volcanology and Geothermal Research 102, 67-95.

Ali, J.R., Thompson, G.M., Zhou, M., Song, X., 2005. Emeishan large igneous province, SW China. Lithos 79, 475 - 489.

Andersen, T., 2002. Correction of common lead in U-Pb analyses that do not report ^{204}Pb. Chemical Geology 192, 59-79.

Betts, P.G., Mason, W.G., Moresi, L., 2012. The influence of a mantle plume head on the dynamics of a retreating subduction zone. Geology 40, 739-742.

Brooks, C.K., Larsen, L.M., Nielsen, T.F.D., 1991. Importance of iron-rich tholeiitic magmas at divergent plate margins: A reappraisal. Geology 19, 269-272.

Campbell, I.H., 2005. Large igneous provinces and the mantle plume hypothesis. Elements 1, 265-269.

Campbell, I.H., Stepanov, A.S., Liang, H., Allen, C.M., Norman, M.D., Zhang, Y., Xie, Y., 2014. The origin of shoshonites: new insights from the tertiary

high-potassium intrusions of eastern Tibet. Contributions to Mineralogy and Petrology 167, 1-22.

Chang, E.Z., 2000. Geology and tectonics of the Songpan-Ganzi fold belt, southwestern China. International Geology Review 42, 813–831.

Chen, J., Xu, J., Ren, J., Huang, X., Wang, B., 2014. Geochronology and geochemical characteristics of late Triassic porphyritic rocks from the Zhongdian arc, eastern Tibet, and their tectonic and metallogenic implications. Gondwana Research 26, 492-504.

Chung, S., Jahn, B., 1995. Plume-lithosphere interaction in generation of the Emeishan flood basalts at the Permian-Triassic boundary. Geology 23, 889-892.

Clague, D.A., Bunch, T.E., 1976. Formation of ferrobasalt at east Pacific midocean spreading centers. Journal of Geophysical Research 81, 4247-4256.

Condie, K.C., 2005. High field strength element ratios in Archean basalts: a window to evolving sources of mantle plumes? Lithos 79, 491-504.

Courtillot, V., Davaille, A., Besse, J., Stock, J., 2003. Three distinct types of hotspots in the Earth's mantle. Earth and Planetary Science Letters 205, 295-308.

Dai, L., Zhao, Z., Zheng, Y., Zhang, J., 2012. The nature of orogenic lithospheric mantle: geochemical constraints from postcollisional mafic–ultramafic rocks in the Dabie orogen. Chemical Geology 334, 99-121.

Dai, L., Zhao, Z., Zheng, Y., Zhang, J., 2015. Source and magma mixing processes in continental subduction factory: geochemical evidence from postcollisional

mafic igneous rocks in the Dabie orogen. Geochemistry, Geophysics, Geosystems 16, 659-680.

Ding, Y., Yang, T.N., Zhang, H.R., Wang, Z.L., Xue, W.W., Zhang, Y.B., 2011. Zircon xenocrysts in diabase dykes, a potential lithosphere probe for the thermo-tectonic evolution of the crust: a case study of zircon xenocrysts of diabase in Yushu mélange. Acta Petrologica et Mineralogica 30, 438-448 (in Chinese with English Abstract) .

Druken, K.A., Kincaid, C., Griffiths, R.W., Stegman, D.R., Hart, S.R., 2014. Plume–slab interaction: the Samoa–Tonga system. Physics of the Earth and Planetary Interiors 232, 1-14.

Duan, Q.F., Wang, J.X., Bai, Y.S., Yao, H.Z., He, L.Q., Zhang, K.X., Kou, X.H., Li, J., 2009. Zircon SHRIMP U-Pb dating and lithogeochemistry of gabbro from the ophiolite in southern Qinghai Province. Geology in China 36, 291-299 (in Chinese with English Abstract) .

Fan, J., Li, C., Wang, M., Xie, C., Xu, W., 2015. Features, provenance, and tectonic significance of carboniferous-Permian glacial marine diamictites in the southern Qiangtang-Baoshan block, Tibetan Plateau. Gondwana Research 28, 1530-1542.

Fan, W., Wang, Y., Zhang, A., Zhang, F., Zhang, Y., 2010. Permian arc–back-arc basin development along the Ailaoshan tectonic zone: geochemical, isotopic and geochronological evidence from the Mojiang volcanic rocks, Southwest China. Lithos 119, 553-568.

Fitton, J.G., Saunders, A.D., Norry, M.J., Hardarson, B.S., Taylor, R.N., 1997. Thermal and chemical structure of the Iceland plume. Earth and Planetary Science Letters 153, 197 - 208.

Fletcher, M., Wyman, D.A., 2015. Mantle plume – subduction zone interactions over the past 60 million years. Lithos 233, 162-173.

Gao, S., Rudnick, R.L., Yuan, H.L., Liu, X.M., Liu, Y.S., Xu, W.L., Ling, W.L., Ayers, J., Wang, X.C., Wang, Q.H., 2004. Recycling lower continental crust in the North China craton. Nature 432, 892-897.

Gazel, E., Hoernle, K., Carr, M.J., Herzberg, C., Saginor, I., den Bogaard, P.v, Hauff, F., Feigenson, M., Swisher, C., 2011. Plume–subduction interaction in southern Central America: mantle upwelling and slab melting. Lithos 121, 117-134.

Gerya, T.V., Stern, R.J., Baes, M., Sobolev, S.V., Whattam, S.A., 2015. Plate tectonics on the Earth triggered by plume-induced subduction initiation. Nature 527, 221-225.

Gibson, S.A., 2002. Major element heterogeneity in Archean to recent mantle plume starting-heads. Earth and Planetary Science Letters 195, 59-74.

Halama, R., Marks, M., Brügmann, G., Siebel, W., Wenzel, T., Markl, G., 2004. Crustal contamination of mafic magmas: evidence from a petrological, geochemical and Sr–Nd–Os–O isotopic study of the Proterozoic Isortoq dike swarm, South Greenland. Lithos 74, 199-232.

Hanan, B.B., Blichert-Toft, J., Kingsley, R., Schilling, J.G., 2000. Depleted Iceland

mantle plume geochemical signature: artifact of multicomponent mixing. Geochemistry, Geophysics, Geosystems 1.

He, B., Xu, Y., Chung, S., Xiao, L., Wang, Y., 2003. Sedimentary evidence for a rapid, kilometer-scale crustal doming prior to the eruption of the Emeishan flood basalts. Earth and Planetary Science Letters 213, 391-405.

He, B., Xu, Y., Huang, X., Luo, Z., Shi, Y., Yang, Q., Yu, S., 2007. Age and duration of the Emeishan flood volcanism, SW China: geochemistry and SHRIMP zircon U – Pb dating of silicici ignimbrites, post-volcanic Xuanwei formation and clay tuff at the Chaotian section. Earth and Planetary Science Letters 255, 306-323.

He, B., Xu, Y., Zhong, Y., Guan, J., 2010a. The Guadalupian–Lopingian boundary mudstones at Chaotian (SW China) are clastic rocks rather than acidic tuffs: implication for a temporal coincidence between the end-Guadalupian mass extinction and the Emeishan volcanism. Lithos 119, 10-19.

He, Q., Xiao, L., Balta, B., Gao, R., Chen, J., 2010b. Variety and complexity of the late-Permian Emeishan basalts: reappraisal of plume--lithosphere interaction processes. Lithos 119, 91-107.

Herzberg, C., Zhang, J., 1996. Melting experiments on anhydrous peridotite KLB-1: compositions of magmas in the upper mantle and transition zone. Journal of Geophysical Research: Solid Earth 101, 8271-8295.

Hu, P., Li, C., Wu, Y., Xie, C., Wang, M., Li, J., 2014. Opening of the Longmu Co, Shuanghu–Lancangjiang ocean: constraints from plagiogranites. Chinese

Science Bulletin 59, 3188-3199.

Jakobsen, J.K., Veksler, I.V., Tegner, C., Brooks, C.K., 2011. Crystallization of the Skaergaard intrusion from an emulsion of immiscible iron- and silica-rich liquids: evidence from melt inclusions in plagioclase. Journal of Petrology 52, 345-373.

Jian, P., Liu, D., Kröner, A., Zhang, Q., Wang, Y., Sun, X., Zhang, W., 2009a. Devonian to Permian plate tectonic cycle of the paleo-Tethys orogen in southwest China (II): insights from zircon ages of ophiolites, arc/back-arc assemblages and within-plate igneous rocks and generation of the Emeishan CFB province. Lithos 113, 767-784.

Jian, P., Liu, D., Kröner, A., Zhang, Q., Wang, Y., Sun, X., Zhang, W., 2009b. Devonian to Permian plate tectonic cycle of the paleo-Tethys orogen in southwest China (I): geochemistry of ophiolites, arc/back-arc assemblages and within-plate igneous rocks. Lithos 113, 748-766.

Kapp, P., Yin, A., Manning, C.E., Harrison, T.M., Taylor, M.H., Ding, L., 2003. Tectonic evolution of the early Mesozoic blueschist-bearing Qiangtang metamorphic belt, central Tibet. Tectonics 22, 540-566.

Kapp, P., Yin, A., Manning, C.E., Murphy, M., Al, E., 2000. Blueschist-bearing metamorphic core complexes in the Qiangtang block reveal deep crustal structure of northern Tibet. Geology 28, 19-22.

Kincaid, C., Druken, K.A., Griffiths, R.W., Stegman, D.R., 2013. Bifurcation of the Yellowstone plume driven by subduction-induced mantle flow. Nature

Geoscience 6, 395-399.

Klemme, S., Günther, D., Hametner, K., Prowatke, S., Zack, T., 2006. The partitioning of trace elements between ilmenite, ulvospinel, armalcolite and silicate melts with implications for the early differentiation of the moon. Chemical Geology 234, 251-263.

Le Roux, V., Dasgupta, R., Lee, C.-A., 2011. Mineralogical heterogeneities in the Earth's mantle: Constraints from Mn, Co, Ni and Zn partitioning during partial melting. Earth and Planetary Science Letters 307, 395-408.

Le Roux, V., Lee, C.-A., Turner, S.J., 2010. Zn/Fe systematics in mafic and ultramafic systems: implications for detecting major element heterogeneities in the Earth’s mantle. Geochimica et Cosmochimica Acta 74, 2779-2796.

Leat, P.T., Riley, T.R., Wareham, C.D., Millar, I.L., Kelley, S.P., Storey, B.C., 2002. Tectonic setting of primitive magmas in volcanic arcs: an example from the Antarctic Peninsula. Journal of the Geological Society 159, 31-44.

Li, C., 1987. The Longmu Co-Shuanghu-Jitang plate suture and the northern boundary of Gondwanaland during carboniferous and Permian. Journal of Changchun Collage of Geology 17, 155-166 (in Chinese with English Abstract) .

Li, C., Huang, X.P., Zhai, Q.G., Zhu, T.X., Yu, Y.S., Wang, G.H., Zeng, Q.G., 2006. The Longmu Co-Shuanghu-Jitang plate suture and the northern boundary of Gondwanaland in the Qinghai-Tibet plateau. Earth Science Frontiers 13, 136-147 (in Chinese with English Abstract).

Li, C., Zhai, Q., Dong, Y., Liu, S., Xie, C., Wu, Y., 2009. High-pressure eclogite-blueschist metamorphic belt and closure of paleo-Tethys Ocean in central Qiangtang, Qinghai-Tibet plateau. Journal of Earth Science 20, 209-218.

Li, C., Zhai, Q.G., Dong, Y.S., Zeng, Q.G., Huang, X.P., 2007. Longmu Co-Shuanghu plate suture in the Qinghai-Tibet Plateau and records of the evolution of the paleo-Tethys Ocean in the Qiangtang area, Tibet, China. Geological Bulletin of China 26, 13-21 (in Chinese with English abstract).

Li, H., Zhang, Z., Santosh, M., Linsu, L., Han, L., Liu, W., Cheng, Z., 2016. Late Permian basalts in the northwestern margin of the Emeishan large igneous Province: implications for the origin of the Songpan-Ganzi terrane. Lithos 256, 75-87.

Li, N., Niu, H., Bao, Z., Shan, Q., Yang, W., Jiang, Y., Zeng, L., 2014. Geochronology and geochemistry of the Paleoproterozoic Fe-rich mafic sills from the Zhongtiao Mountains: petrogenesis and tectonic implications. Precambrian Research 255, 668-684.

Liu, B., Ma, C.Q., Guo, Y.H., Xiong, F.H., Guo, P., Zhang, X. , 2016a. Petrogenesis and tectonic implications of Triassic mafic complexes with MORB/OIB affinities from the western Garzê-Litang ophiolitic mélange, central Tibetan Plateau. Lithos 260, 253-267.

Liu, B., Ma, C.Q., Huang, J., Xiong, F.H., Zhang, X., Guo, Y.H., 2016b. Petrogenetic mechanismand tectonic significance of Triassic Yushu volcanic rocks in the

northern part of thenorth Qiangtang terrane. Acta Petrologica et Mineralogica 35, 1–15 (in Chinese with English Abstract).

Liu, Y., Gao, S., Hu, Z., Gao, C., Zong, K., Wang, D., 2010a. Continental and oceanic crust recycling-induced melt-peridotite interactions in the trans-North China orogen: U--Pb dating, Hf isotopes and trace elements in zircons from mantle xenoliths. Journal of Petrology 51, 537-571.

Liu, Y., Hu, Z., Gao, S., Günther, D., Xu, J., Gao, C., Chen, H., 2008a. *In situ* analysis of major and trace elements of anhydrous minerals by LA-ICP-MS without applying an internal standard. Chemical Geology 257, 34--43.

Liu, Y., Hu, Z., Zong, K., Gao, C., Gao, S., Xu, J., Chen, H., 2010b. Reappraisement and refinement of zircon U-Pb isotope and trace element analyses by LA-ICP-MS. Chinese Science Bulletin 55, 1535-1546.

Liu, Y., Zong, K., Kelemen, P.B., Gao, S., 2008b. Geochemistry and magmatic history of eclogites and ultramafic rocks from the Chinese continental scientific drill hole: subduction and ultrahigh-pressure metamorphism of lower crustal cumulates. Chemical Geology 247, 133-153.

Loucks, R.R., 1990. Discrimination of ophiolitic from nonophiolitic ultramafic-mafic allochthons in orogenic belts by the Al/Ti ratio in clinopyroxene. Geology 18, 346-349.

Lu, Y.F., 2004. Geokit—a geochemical toolkit for Microsoft Excel. Geochimica 33, 459-464 (in Chinese with English Abstract).

Ludwing, K.R., 2003. Users Manual for Isoplot 3.00: A Geochronological Toolkit for

Microsoft Excel. Ex. Rev 2, 1-56.

McKenzie, D., O'Nions, R.K., 1991. Partial melt distributions from inversion of rare earth element concentrations. Journal of Petrology 32, 1021-1091.

Metcalfe, I., 2013. Gondwana dispersion and Asian accretion: tectonic and palaeogeographic evolution of eastern Tethys. Journal of Asian Earth Sciences 66, 1-33.

Montelli, R., Nolet, G., Dahlen, F.A., Masters, G., 2006. A catalogue of deep mantle plumes: New results from finite-frequency tomography. Geochemistry, Geophysics, Geosystems 7.

Morgan, J.W., 1972. Deep mantle convection plumes and plate motions. AAPG Bulletin 56, 203-213.

Morimoto, N., 1988. Nomenclature of pyroxenes. Mineralogy and Petrology 39, 55-76.

Murray, K.E., Ducea, M.N., Schoenbohm, L., 2015. Foundering-driven lithospheric melting: the source of central Andean mafi c lavas on the Puna Plateau (22°S-27°S). The Geological Society of America Memoir 212, 139-166.

Naumann, T.R., Geist, D.J., 1999. Generation of alkalic basalt by crystal fractionation of tholeiitic magma. Geology 27, 423-426.

Nie, S., Yin, A., Rowley, D.B., Jin, Y., 1994. Exhumation of the Dabie Shan ultra-high-pressure rocks and accumulation of the Songpan-Ganzi Flysch sequence, central China. Geology 22, 999-1002.

Nielsen, R.L., Beard, J.S., 2000. Magnetite-melt HFSE partitioning. Chemical

Geology 164, 21-34.

Niu, Y., O'Hara and M.J., 2003. Origin of ocean island basalts: A new perspective from petrology, geochemistry, and mineral physics considerations. Journal of Geophysical Research 108, 1-19.

Pan, G., Wang, L., Li, R., Yuan, S., Ji, W., Yin, F., Zhang, W., Wang, B., 2012. Tectonic evolution of the Qinghai-Tibet plateau. Journal of Asian Earth Sciences 53, 3-14.

Pang, K., Li, C., Zhou, M., Ripley, E.M., 2009. Mineral compositional constraints on petrogenesis and oxide ore genesis of the late Permian Panzhihua layered gabbroic intrusion, SW China. Lithos 110, 199-214.

Pearce, J.A., 2008. Geochemical fingerprinting of oceanic basalts with applications to ophiolite classification and the search for Archean oceanic crust. Lithos 100, 14-48.

Pearce, J.A., Baker, P.E., Harvey, P.K., Luff, I.W., 1995. Geochemical evidence for subduction fluxes, mantle melting and fractional crystallization beneath the south sandwich island arc. Journal of Petrology 36, 1073-1109.

Peng, T., Wilde, S.A., Fan, W., Peng, B., Mao, Y., 2013. Mesoproterozoic high Fe-Ti mafic magmatism in western Shandong, North China Craton: petrogenesis and implications for the final breakup of the Columbia supercontinent. Precambrian Research 235, 190-207.

Peng, T., Zhao, G., Fan, W., Peng, B., Mao, Y., 2014. Zircon geochronology and Hf isotopes of Mesozoic intrusive rocks from the Yidun terrane, Eastern Tibetan

Plateau: petrogenesis and their bearings with Cu mineralization. Journal of Asian Earth Sciences 80, 18-33.

Perfit, M.R., Fornari, D.J., Malahoff, A., Embley, R.W., 1983. Geochemical studies of abyssal lavas recovered by DSRV Alvin from eastern Galapagos rift. Inca Transform, and Ecuador Rift 2, 10530-10550.

Pullen, A., Kapp, P., Gehrels, G.E., Vervoort, J.D., Ding, L., 2008. Triassic continental subduction in central Tibet and Mediterranean-style closure of the paleo-Tethys Ocean. Geology 36, 351-354.

Reid, A.J., Wilson, C.J.L., Liu, S., 2005. Structural evidence for the Permo-Triassic tectonic evolution of the Yidun arc, eastern Tibetan Plateau. Journal of Structural Geology 27, 119-137.

Saccani, E., Azimzadeh, Z., Dilek, Y., Jahangiri, A., 2013. Geochronology and petrology of the early carboniferous Misho mafic complex (NW Iran), and implications for the melt evolution of paleo-Tethyan rifting in western Cimmeria. Lithos 162-163, 264-278.

Shellnutt, J.G., 2014. The Emeishan large igneous province: A synthesis. Geoscience Frontiers 5, 369-394.

Song, X.Y., Zhou, M.F., Cao, Z.M., Robinson, P.T., 2004. Late Permian rifting of the South China Craton caused by the Emeishan mantle plume? Journal of the Geological Society 161, 773-781.

Sun, S.S., McDonough, W.F., 1989. Chemical and isotopic systematics of oceanic basalts: mplications for mantle composition and processes. Geological Society,

London, Special Publications 42, 313-345.

Tatsumi, Y., Eggins, S., 1995. Subduction Zone Magmatism. Blackwell Publishing House Science, Cambridge, pp. 1-211.

Taylor, S.R., McLennan, S.M., 1985. The Continental Crust: Its Composition and Evolution. Blackwell Scientific Publications, Oxford, pp.1-328.

Turner, S., Hawkesworth, C., 1998. Using geochemistry to map mantle flow beneath the Lau Basin. Geology 26, 1019-1022.

Volkert, R.A., Feigenson, M.D., Mana, S., Bolge, L., 2015. Geochemical and Sr–Nd isotopic constraints on the mantle source of Neoproterozoic mafic dikes of the rifted eastern Laurentian margin, north-central Appalachians, USA. Lithos 212-215, 202-213.

Wang, B., Zhou, M., Li, J., Yan, D., 2011. Late Triassic porphyritic intrusions and associated volcanic rocks from the Shangri-la region, Yidun terrane, Eastern Tibetan Plateau: Adakitic magmatism and porphyry copper mineralization. Lithos 127, 24-38.

Wang, X., Metcalfe, I., Jian, P., He, L., Wang, C., 2000. The Jinshajiang–Ailaoshan suture Zone, China: tectonostratigraphy, age and evolution. Journal of Asian Earth Sciences 18, 675-690.

Wang, Y., Zhang, A., Fan, W., Zhang, Y., Zhang, Y., 2013. Origin of paleosubduction-modified mantle for Silurian gabbro in the Cathaysia block: geochronological and geochemical evidence. Lithos 160–161, 37-54.

Wang, Y., Zhao, G., Cawood, P.A., Fan, W., Peng, T., Sun, L., 2008. Geochemistry of

Paleoproterozoic (~1770Ma) mafic dikes from the trans-North China orogen and tectonic implications. Journal of Asian Earth Sciences 33, 61-77.

Weaver, B.L., 1991. The origin of Ocean Island basalt end-member compositions: trace element and isotopic constraints. Earth and Planetary Science Letters 104, 381-397.

Weislogel, A.L., 2008. Tectonostratigraphic and geochronologic constraints on evolution of the northeast Paleotethys from the Songpan-Ganzi complex, central China. Tectonophysics 451, 331–345.

Whattam, S.A., Stern, R.J., 2015. Late Cretaceous plume-induced subduction initiation along the southern margin of the Caribbean and NW South America: the first documented example with implications for the onset of plate tectonics. Gondwana Research 27, 38-63.

Winchester, J.A., Floyd, P.A., 1977. Geochemical discrimination of different magma series and their differentiation products using immobile elements. Chemical Geology 20, 325-343.

Wu, Y.W., Li, C., Xie, C.M., Wang, M., Peiyuan, H., 2013. Petrology, geochemistry and tectonic significance of the metamorphic peridotites from Longmuco-Shuanghu ophiolitic melange belt, Tibet. Acta Geologica Sinica (English Edition) 87, 426-439.

Xiao, L., He, Q., Pirajno, F., Ni, P., Du, J., Wei, Q., 2008. Possible correlation between a mantle plume and the evolution of paleo-Tethys Jinshajiang Ocean: evidence from a volcanic rifted margin in the Xiaru-Tuoding area, Yunnan,

SW China. Lithos 100, 112-126.

Xiao, L., Xu, Y.G., Mei, H.J., Zheng, Y.F., He, B., Pirajno, F., 2004. Distinct mantle sources of low-Ti and high-Ti basalts from the western Emeishan large igneous province, SW China: implications for plume--lithosphere interaction. Earth and Planetary Science Letters 228, 525-546.

Xiao, L., Zhang, H.F., Clemens, J.D., Wang, Q.W., Kan, Z.Z., Wang, K.M., Ni, P.Z., Liu, X.M., 2007. Late Triassic granitoids of the eastern margin of the Tibetan Plateau: geochronology, petrogenesis and implications for tectonic evolution. Lithos 96, 436-452.

Xu, Y., Chung, S., Jahn, B., Wu, G., 2001. Petrologic and geochemical constraints on the petrogenesis of Permian–Triassic Emeishan flood basalts in southwestern China. Lithos 58, 145-168.

Xu, Y., He, B., Chung, S., Menzies, M.A., Frey, F.A., 2004. Geologic, geochemical, and geophysical consequences of plume involvement in the Emeishan flood-basalt province. Geology 32, 917.

Xu, Z.Q., Yang, J.S., Li, W.C., Li, H.Q., Cai, Z.H., Yan, Z., Ma, C.Q., 2013. Paleo-Tethys system and accretionary orogen in the Tibetan Plateau. Acta Petrologica Sinica 29, 1847-1860 (in Chinese with English Abstract).

Yang, T.N., Ding, Y., Zhang, H.R., Fan, J.W., Liang, M.J., Wang, X.H., 2014. Two-phase subduction and subsequent collision defines the Paleotethyan tectonics of the southeastern Tibetan Plateau: evidence from zircon U-Pb dating, geochemistry, and structural geology of the Sanjiang orogenic belt,

southwest China. Geological Society of America Bulletin 126, 1654-1682.

Yang, T.N., Hou, Z.Q., Wang, Y., Zhang, H.R., Wang, Z.L., 2012. Late Paleozoic to early Mesozoic tectonic evolution of northeast Tibet: evidence from the Triassic composite western Jinsha-Garzê-Litang suture. Tectonics 31, 1-20.

Yang, T.N., Zhang, H.R., Liu, Y.X., Wang, Z.L., Song, Y.C., Yang, Z.S., Tian, S.H., Xie, H.Q., Hou, K.J., 2011. Permo-Triassic arc magmatism in central Tibet: evidence from zircon U–Pb geochronology, Hf isotopes, rare earth elements, and bulk geochemistry. Chemical Geology 284, 270-282.

Yin, A., Harrison, T.M., 2000. Geologic evolution of the Himalayan-Tibetan orogen. Annual Review of Earth and Planetary Science 28, 211-280.

Yong, Y., Chen, W., Zhang, Y., Liu, X.Y., 2011. Zircon SHRIMP U-Pb dating and geochemistry of the Rangnianggongba gabbro in Yushu area,Qinghai Province. Acta Petrologica et Mineralogica 30, 419-426 (in Chinese with English Abstract).

Zhai, Q., Jahn, B., Wang, J., Su, L., Mo, X., Wang, K., Tang, S., Lee, H., 2013. The carboniferous ophiolite in the middle of the Qiangtang terrane, Northern Tibet: SHRIMP U–Pb dating, geochemical and Sr–Nd–Hf isotopic characteristics. Lithos 168–169, 186-199.

Zhai, Q., Zhang, R., Jahn, B., Li, C., Song, S., Wang, J., 2011. Triassic eclogites from central Qiangtang, northern Tibet, China: petrology, geochronology and metamorphic P–T path. Lithos 125, 173-189.

Zhai, Q.G., Li, C., Wang, J., Chen, W., Zhang, Y., 2009. Petrology, mineralogy and

$^{40}Ar/^{39}Ar$ chronology for Rongma blueschist from central Qiangtang, northern Tibet. Acta Petrologica Sinica 25, 2281-2288 (in Chinese with English Abstract).

Zhang, H.F., Parrish, R., Zhang, L., Xu, W.C., Yuan, H., Gao, S., Crowley, Q.G., 2007. A-type granite and adakitic magmatism association in Songpan–Garze fold belt, eastern Tibetan Plateau: implication for lithospheric delamination. Lithos 97, 323-335.

Zhang, N., Li, J.B., Yang, Y.S., Na, F.C., 2012. Petrogeochemical characteristics and tectonic setting of the Wandaohu ophiolite melange, Jinshajiang suture, Tibet. Acta Petrologica Sinica 28, 1291-1304 (in Chinese with English Abstract).

Zhao, J., Zhou, M., 2007. Geochemistry of Neoproterozoic mafic intrusions in the Panzhihua district (Sichuan Province, SW China): implications for subduction-related metasomatism in the upper mantle. Precambrian Research 152, 27-47.

Zhao, J., Zhou, M., 2009. Secular evolution of the Neoproterozoic lithospheric mantle underneath the northern margin of the Yangtze block, South China. Lithos 107, 152-168.

Zhao, Z.F., Dai, L.Q., Zheng, Y.F., 2013. Postcollisional mafic igneous rocks record crust-mantle interaction during continental deep subduction. Scientific Reports 3, 3413.

Zheng, S., Hu, Z.C., Shi, Y.F., 2009. Accurate determination of Ni, Ca and Mn in olivine by EPMA and LA-ICP-MS. Journal of China University of

Geosciences 34, 220-224 (in Chinese with English Abstract).

Zhou, M., Malpas, J., Song, X., Robinson, P.T., Sun, M., Kennedy, A.K., Lesher, C.M., Keays, R.R., 2002. A temporal link between the Emeishan large igneous province (SW China) and the end-Guadalupian mass extinction. Earth and Planetary Science Letters 196, 113 - 122.

Zhou, M., Zhao, J., Qi, L., Su, W., Hu, R., 2006. Zircon U-Pb geochronology and elemental and Sr–Nd isotope geochemistry of Permian mafic rocks in the Funing area, SW China. Contributions to Mineralogy and Petrology 151, 1-19.

Zhou, M.F., Robinson, P.T., Lesher, C.M., Keays, R.R., Zhang, C., Malpas, J., 2005. Geochemistry, petrogenesis and Metallogenesis of the Panzhihua gabbroic layered intrusion and associated Fe-Ti-V oxide deposits, Sichuan Province, SW China. Journal of Petrology 46, 2253-2280.

Zi, J.W., Cawood, P.A., Fan, W.M., Wang, Y., Tohver, E., McCuaig, T.C., Peng, T.P., 2012. Triassic collision in the paleo-Tethys Ocean constrained by volcanic activity in SW China. Lithos 144–145, 145-160.

Zi, J.W., Cawood, P.A., Fan, W.M., Tohver, E., Wang, Y., McCuaig, T.C., Peng, T.P., 2013. Late Permian-Triassic magmatic evolution in the Jinshajiang orogenic belt, SW China and implications for orogenic processes following closure of the paleo-Tethys. American Journal of Science 313, 81-112.

Zi, J.W., Fan, W.M., Wang, Y.J., Cawood, P.A., Peng, T.P., Sun, L.H., Xu, Z.Q., 2010. U-Pb geochronology and geochemistry of the Dashibao basalts in the Songpan-Ganzi terrane, SW China, with implications for the age of Emeishan

volcanism. American Journal of Science 310, 1054-1080.

Figure captions

Fig. 1 The location of the Tibetan Plateau and the Emeishan large igneous province (a; after Yang et al., 2011; Shellnutt, 2014) and simplified geological map of the Yushu area (b).

Fig. 2 Photomicrographs of the four representative mafic rocks in the Yushu area. (a), Yushu gabbro; (b), Haxiu gabbro; (c), Zhiduo dolerite; (d), Zhiduo gabbro; Bt, biotite; Cpx, clinopyroxene; Gt, garnet; Hb, hornblende; Opa, opaque minerals; Pl, plagioclase.

Fig. 3 CL images (a) and LA-ICP-MS U-Pb concordant diagrams (b) of zircon grains for the Yushu mafic rocks.

Fig. 4 Zr/TiO_2-Nb/Y (Winchester and Floyd, 1977) and $(CaO+Al_2O_3)$-(FeO_t+TiO_2)-MgO (Zhou et al.2005) plots for the Yushu mafic rocks. Data for the HT and LT (Emeishan high-Ti and low-Ti basalts) are from He et al. (2010b), Xiao et al. (2004) and Xu et al.(2001); Data for Funing high-Ti mafic intrusion are from Zhou et al.(2006); Data for Fe-Ti-rich mafic rocks are from Aden and Frizzo (1996), Brooks et al.(1991) and Zhou et al.(2005).

Fig. 5 Chondrite-normalized REE distribution patterns (a,c,e) and primitive mantle-normalized trace element spider diagrams (b,e,f) for the Yushu mafic rocks. Data for chondrite are from Taylor and Mclennan (1985); Data for primitive mantle and OIB are from Sun and McDonough (1989); Data for IAT (Island arc tholeiitic basalts) compositions are from Niu and O'Hara (2003); Data for the HT and LT are from He et al. (2010b), Xiao et al. (2004) and Xu et

al.(2001); Data for Funing high-Ti mafic intrusion are from Zhou et al.(2006); Data for primitive mafic melts derived from subduction-modified lithospheric and asthenospheric mantle are from Leat et al. (2002).

Fig. 6 Plot of $\varepsilon_{Nd}(t)$ vs. I_{sr} and $\varepsilon_{Nd}(t)$ vs. $Mg^{\#}$ for the Yushu mafic rocks. Data for the HT and LT (Xu et al., 2001; Xiao et al., 2004; He et al., 2010) and Funing high-Ti mafic intrusion (Zhou et al., 2006) are shown for comparision. The fields for MORB, OIB, BSE, HIMU, EMI and EMII are from Hart (1988) and Weaver (1991).

Fig. 7 Plots of Wo-En-Fs (Morimoto, 1988) and Al_z (in percent of total tetrahedral cations) vs. TiO_2 (Loucks, 1990) for the pyroxenes of the Group 1 rocks. Data for clinopyroxenes of the Panzhihua mafic-ultramafic rocks are from Pang et al. (2009).

Fig. 8 Plots of TiO_2, FeO_t, CaO, P_2O_5, Cr, Ni, CaO/Al_2O_3, Sc/Y, Nb/La vs. $Mg^{\#}$ for the Yushu mafic rocks.

Fig. 9 Plots of Nb/La vs. TiO_2 and Nb/Y vs. Zr/Y (Condie, 2005) for the Yushu mafic rocks. Data for the HT and LT are from He et al. (2010b), Xiao et al. (2004) and Xu et al. (2001); Data for Funing high-Ti mafic intrusion are from Zhou et al.(2006).

Fig. 10 Plots of Th/Yb vs. Nb/Yb (Pearce, 2008) and Nb/U vs. Nb for the Yushu mafic rocks. Data for South Sandwich arc are from Pearce et al. (1995); Data for primitive mafic melts derived from subduction-modified lithospheric and asthenospheric mantle are from Leat et al. (2002); Data for the HT and LT are

from He et al. (2010b), Xiao et al. (2004) and Xu et al. (2001); Data for Funing high-Ti mafic intrusion are from Zhou et al. (2006).

Fig. 11 Zn/Fe_t ($\times 10^4$) vs. MgO and Sm/Yb vs. La/Yb diagrams for the Yushu mafic rocks. Melting curves in Fig. 11b is after Zhao and Zhou (2009).

Fig. 12 Schematic illustration for the geodynamic setting and generation of the Yushu mafic rocks.

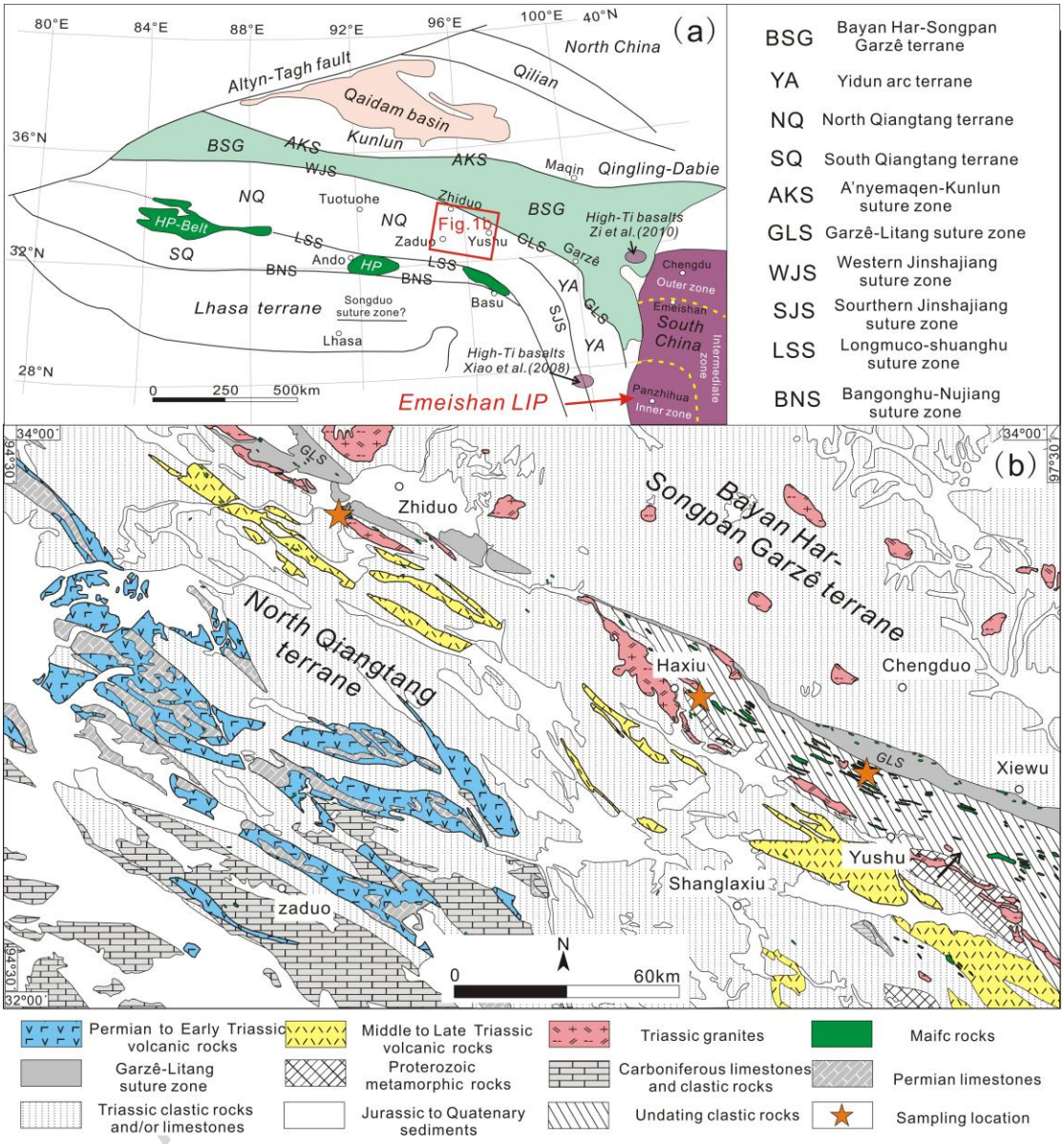

Figure 1

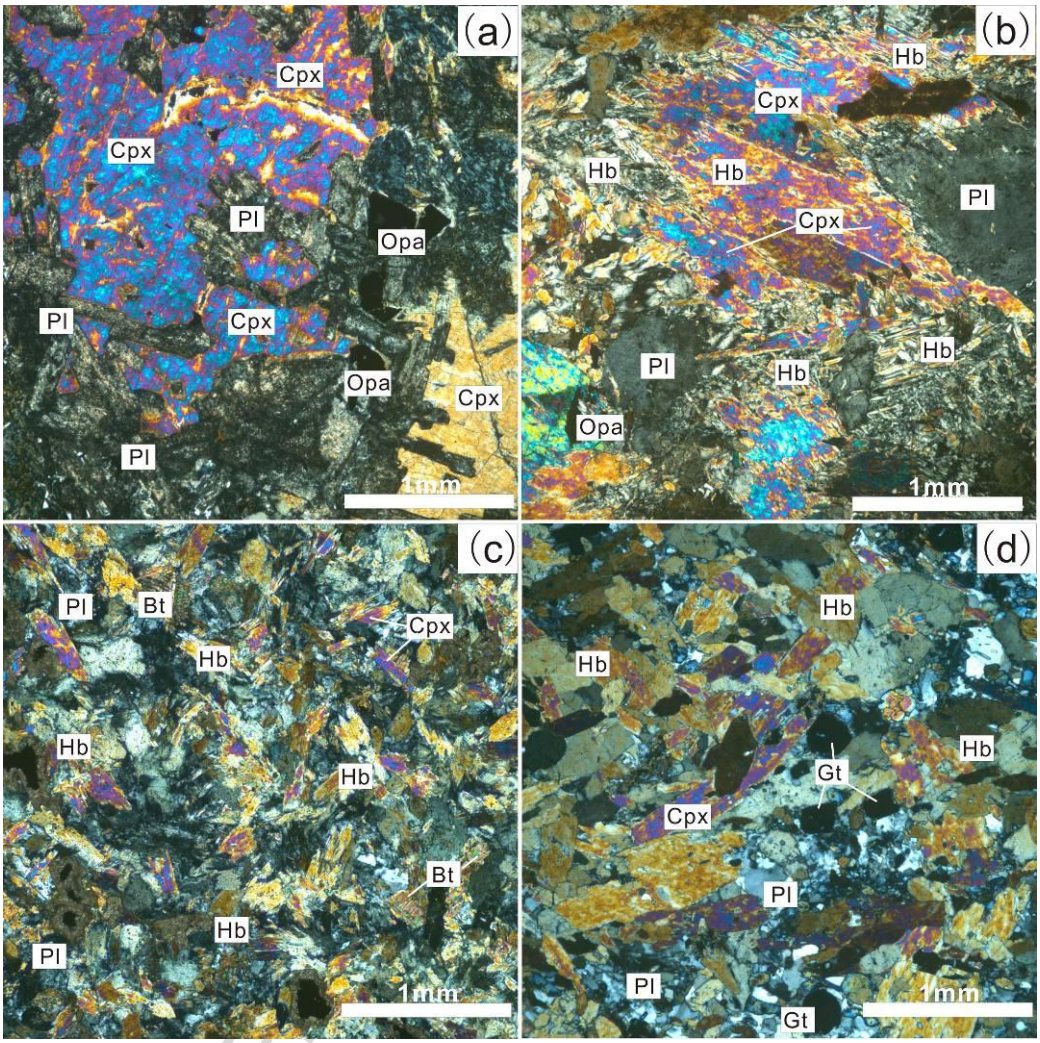

Figure 2

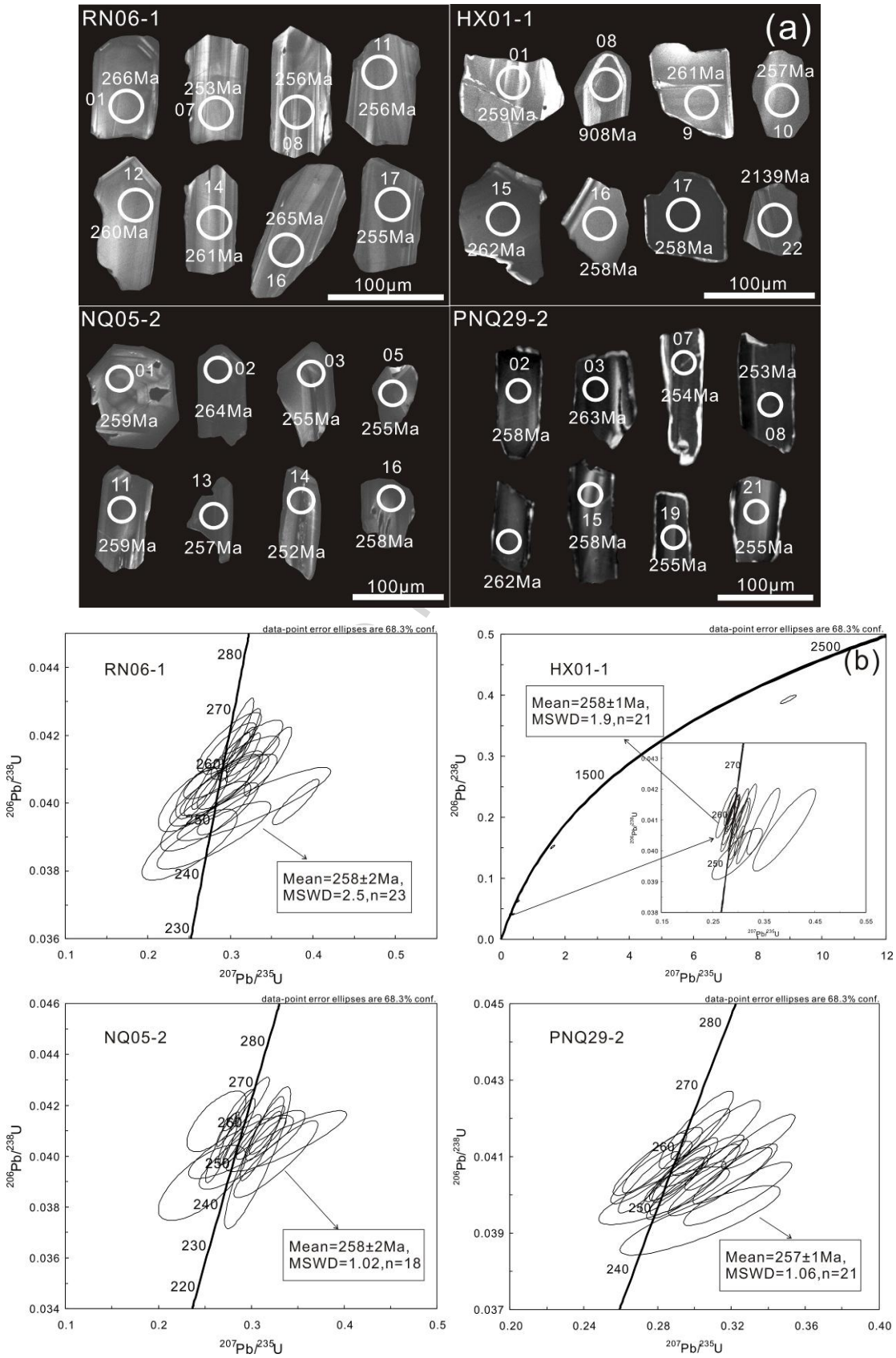

Figure 3

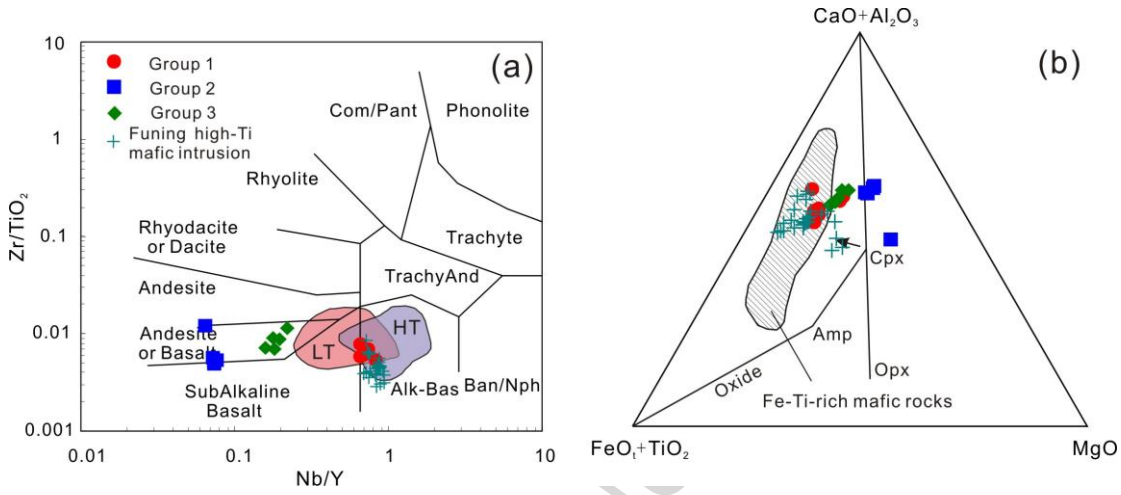

Figure 4

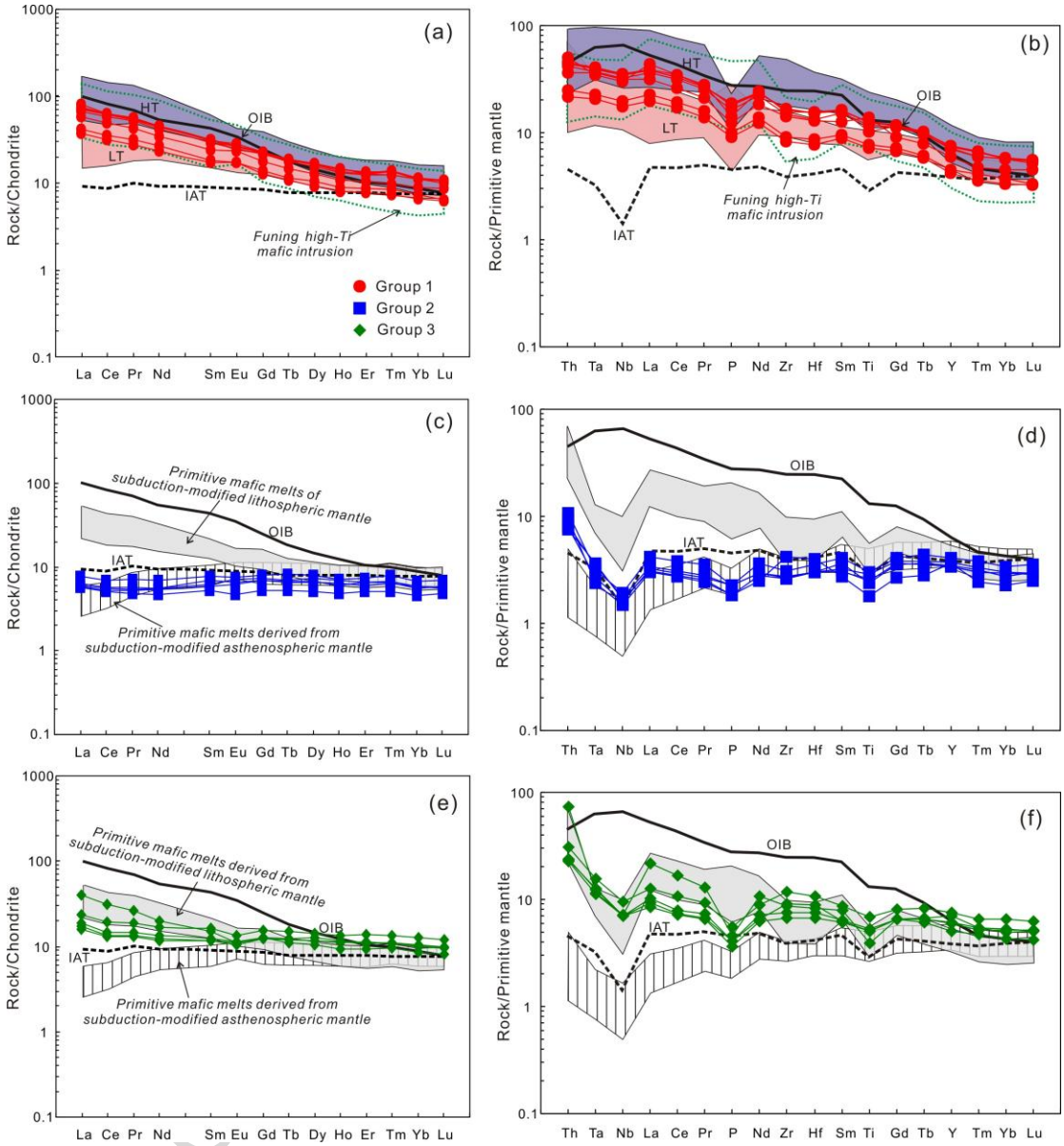

Figure 5

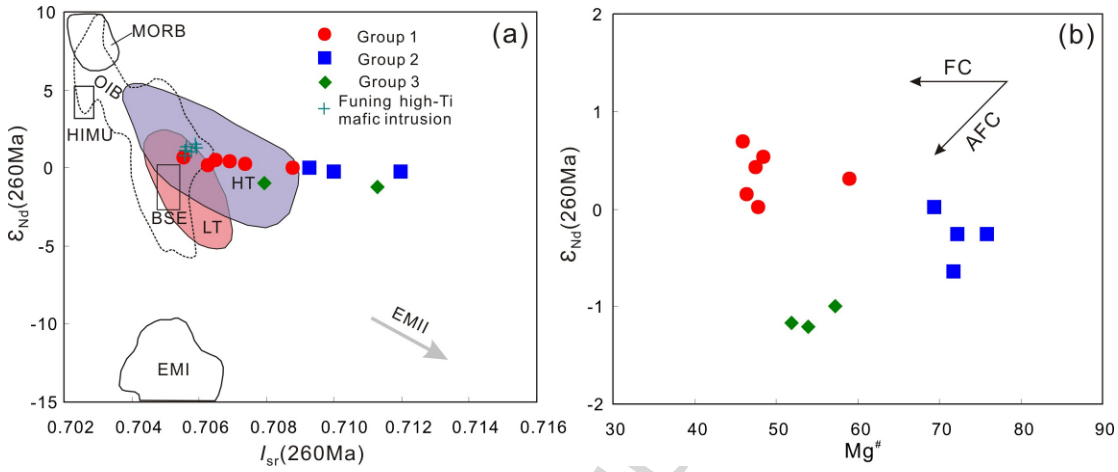

Figure 6

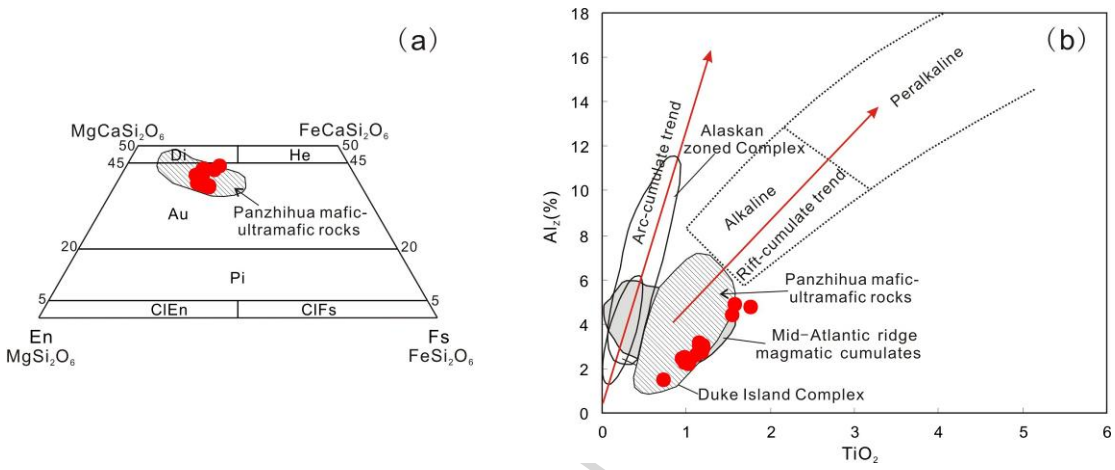

Figure 7

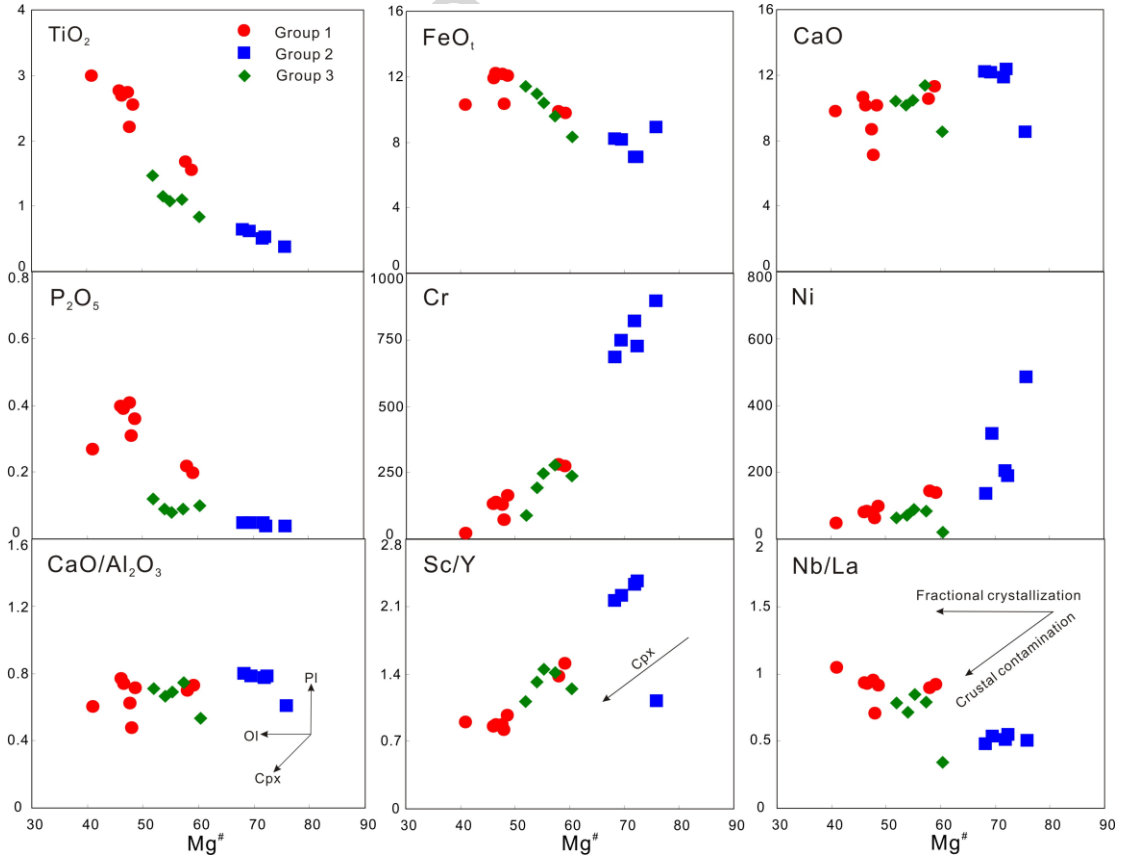

Figure 8

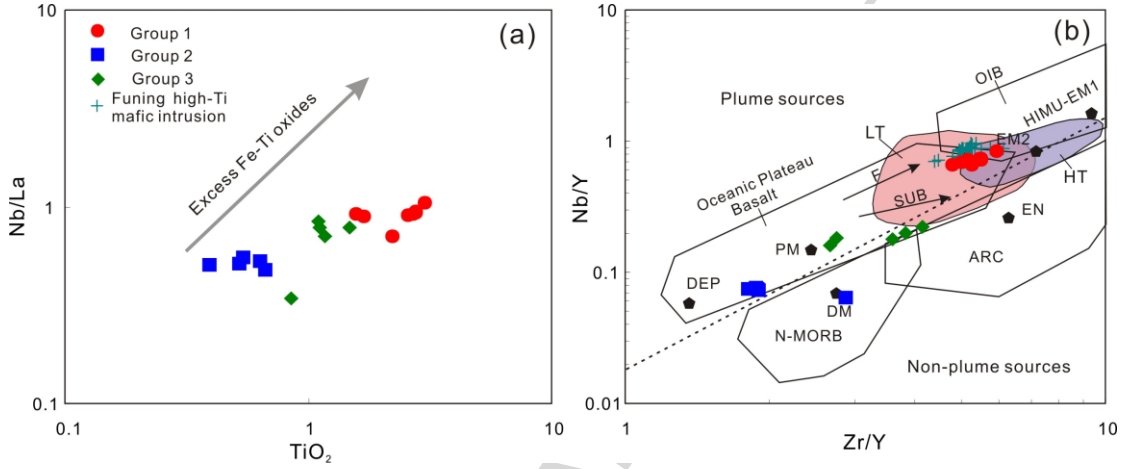

Figure 9

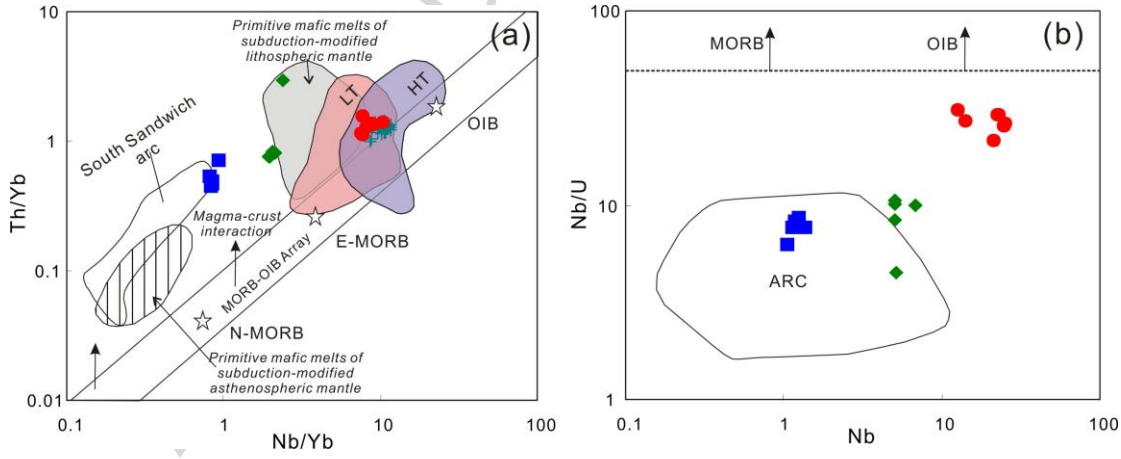

Figure 10

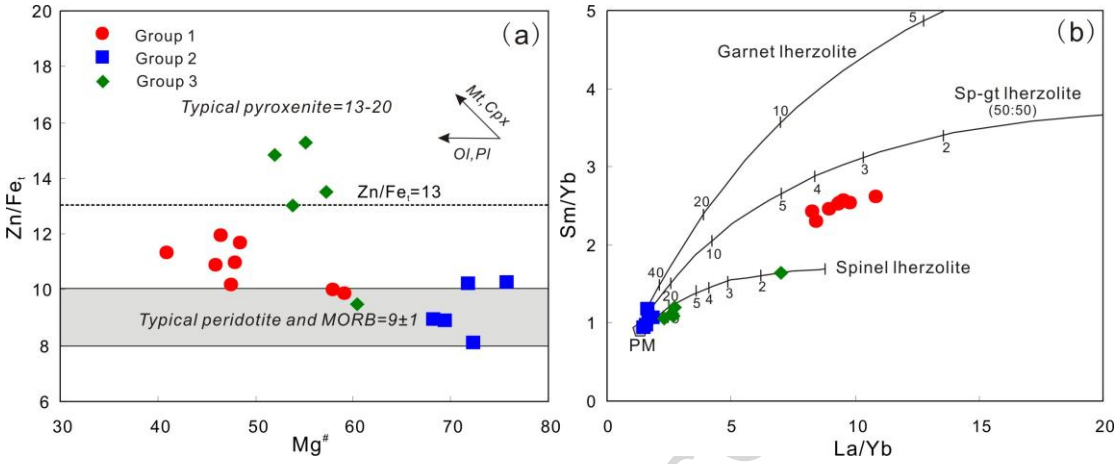

Figure 11

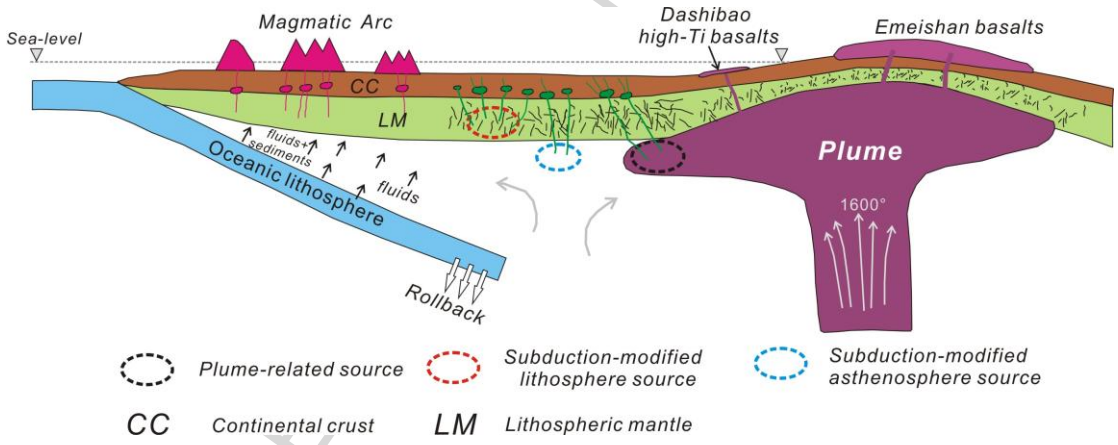

Figure 12

Table 1 Major (in wt.%) , trace element (in ppm) and Sr-Nd isotopic compositions of the Yushu mafic rocks

Rocks	Yushu gabbros (Group 1)					Zhiduo dolerites (Group 1)			Haxiu gabbros (Group 2)					Zhiduo gabbros (Group 3)				
Sample no.	YS30-3	YS31-4	YS31-5	RN06-1	RN06-2	DC03-1	DC04-1	DC05-1	HX01-1	HX02-1	HX03-1	HX05-1	HX05-2	PNG29-2	PNQ29-1	NQ15-3	NQ15-4	DC50-1
SiO_2	48.13	48.37	48.17	51.40	49.04	48.02	48.50	48.47	45.30	48.53	48.78	50.34	48.75	49.41	49.05	49.89	49.75	53.42
TiO_2	2.77	2.70	2.75	2.22	3.00	1.56	2.56	1.69	0.39	0.63	0.54	0.52	0.66	1.48	1.16	1.11	1.09	0.85
Al_2O_3	13.79	13.71	13.81	14.84	16.19	15.44	14.09	15.04	13.91	15.46	15.71	15.29	15.16	14.68	15.16	15.18	15.14	15.85
Fe_2O_3	2.55	3.11	2.15	1.68	2.62	1.57	2.38	0.92	1.24	0.97	0.88	0.27	1.38	2.33	2.17	1.81	1.60	1.35
FeO	9.60	9.40	10.25	8.82	7.92	8.40	9.90	9.07	7.82	7.28	6.35	6.88	6.98	9.30	9.02	7.97	8.98	7.13
FeOt	11.89	12.20	12.18	10.33	10.28	9.81	12.04	9.90	8.94	8.15	7.14	7.12	8.22	11.40	10.97	9.60	10.42	8.34
MnO	0.20	0.20	0.20	0.21	0.17	0.16	0.20	0.17	0.16	0.15	0.13	0.13	0.15	0.23	0.21	0.18	0.20	0.14
MgO	5.67	5.92	6.19	5.31	3.98	7.94	6.35	7.64	15.67	10.38	10.44	10.16	9.90	6.90	7.19	7.22	7.19	7.14
CaO	10.67	10.15	8.67	7.10	9.78	11.30	10.13	10.54	8.53	12.16	12.37	11.86	12.20	10.42	10.13	11.37	10.45	8.51
Na_2O	2.41	2.13	3.61	4.85	3.54	2.37	2.81	2.78	1.61	1.86	1.84	1.79	1.68	2.38	2.47	2.25	2.87	2.02
K_2O	1.04	0.95	0.73	0.35	0.78	0.39	0.77	0.42	0.20	0.20	0.31	0.33	0.36	0.65	0.67	0.47	0.50	1.23
P_2O_5	0.40	0.39	0.41	0.31	0.27	0.20	0.36	0.22	0.04	0.05	0.04	0.05	0.05	0.12	0.09	0.09	0.08	0.10
CO_2	0.08	0.06	0.10	0.09	0.20	0.12	0.08	0.33	0.50	0.05	0.13	0.02	0.05	0.08	0.34	0.35	0.31	0.10
H_2O^+	2.46	2.69	2.76	2.67	2.28	2.34	1.68	2.49	4.38	2.04	2.26	2.15	2.45	1.85	2.04	1.91	1.64	1.99
Total	99.77	99.78	99.80	99.85	99.77	99.81	99.81	99.78	99.75	99.76	99.78	99.79	99.77	99.83	99.70	99.80	99.80	99.83
Sc	29.2	29.8	29.7	27.1	24.4	29.1	31.0	28.3	18.4	37.7	36.7	37.0	40.2	38.3	41.8	39.7	39.7	28.9
V	317	321	317	290	403	260	326	258	131	255	199	202	236	364	318	270	284	221
Cr	132.6	137.6	130.6	73.8	21.8	274.7	162.6	279.7	895.5	747.5	726.9	821.4	684.4	89.46	192.6	276.7	247.6	237.9
Co	58.7	56.7	56.8	61.0	65.7	56.2	63.7	56.5	87.5	81.5	69.5	64.0	63.1	58.3	59.7	67.8	74.2	65.2

Ni	83.7	86.2	83.5	66.3	50.8	140.7	100.2	145.6	486.0	318.8	192.0	205.7	138.4	65.4	72.6	86.1	91.2	23.1
Cu	118.6	117.9	110.9	63.7	109.8	63.8	118.4	88.2	46.3	185.1	57.2	53.8	208.9	140.6	63.9	69.1	35.2	17.1
Zn	101.0	113.8	96.9	88.7	90.9	75.6	109.7	77.4	71.6	56.6	45.3	57.0	57.4	131.8	111.2	100.9	123.9	61.7
Ga	23.0	21.8	24.9	18.7	23.5	19.1	21.5	19.4	12.6	15.0	14.5	14.7	15.1	19.8	18.4	17.2	17.4	18.7
Rb	25.7	24.8	16.0	9.2	19.0	10.0	23.6	9.6	4.8	4.3	10.4	5.1	10.1	15.7	17.3	11.5	11.2	56.3
Sr	547	577	360	199	448	447	389	631	114	122	168	137	149	137	135	162	139	150
Y	34.1	34.1	33.9	32.9	27.1	19.2	32.0	20.5	16.4	17.0	15.5	15.9	18.6	34.4	31.7	28.1	27.5	23.1
Zr	188	187	185	174	160	92	165	102	47	31	29	30	35	133	85	101	76	96
Nb	24.7	25.1	24.9	21.4	22.6	12.6	22.8	14.0	1.1	1.3	1.2	1.1	1.4	6.8	5.1	5.0	5.0	5.1
Cs	0.3	0.4	0.2	0.7	0.8	0.4	1.1	0.2	1.1	0.4	1.0	0.3	1.9	0.2	0.3	0.5	0.5	1.0
Ba	331	258	220	134	206	127	220	206	37	40	45	37	58	72	60	73	70	269
La	26.4	27.1	26.1	30.3	21.5	13.7	24.9	15.6	2.1	2.3	2.1	2.2	2.9	8.7	7.1	6.4	5.9	15.0
Ce	58.4	61.0	58.4	61.3	46.9	30.6	55.5	34.2	4.9	5.5	5.0	5.2	6.7	18.9	14.1	13.2	12.7	30.0
Pr	7.4	7.7	7.5	7.8	5.9	3.8	7.1	4.4	0.7	0.8	0.7	0.7	1.0	2.6	2.0	1.9	1.8	3.6
Nd	31.9	31.7	32.2	32.8	24.8	16.7	30.2	19.0	3.4	4.0	3.8	3.9	5.0	12.0	9.7	8.9	8.5	14.5
Sm	7.12	7.30	7.06	7.31	5.55	3.99	6.84	4.24	1.21	1.44	1.36	1.61	1.82	3.85	2.87	2.75	2.70	3.52
Eu	2.30	2.34	2.45	2.10	2.03	1.49	2.17	1.51	0.41	0.62	0.55	0.56	0.66	1.19	1.00	0.98	0.92	0.98
Gd	6.90	7.03	6.99	6.81	5.48	3.97	6.63	4.24	1.62	2.27	2.15	2.13	2.43	4.77	3.91	3.88	3.87	3.89
Tb	1.09	1.09	1.10	1.06	0.85	0.63	1.05	0.67	0.31	0.41	0.38	0.40	0.47	0.89	0.73	0.72	0.71	0.65
Dy	6.50	6.34	6.38	6.22	4.89	3.55	5.94	3.99	1.96	2.80	2.53	2.58	3.04	5.55	4.89	4.57	4.47	4.02
Ho	1.25	1.23	1.24	1.16	0.93	0.69	1.12	0.76	0.41	0.59	0.54	0.52	0.61	1.16	1.01	0.97	0.96	0.80
Er	3.27	3.35	3.22	3.20	2.60	1.94	3.11	2.15	1.27	1.63	1.52	1.65	1.80	3.44	2.82	2.71	2.85	2.34
Tm	0.49	0.49	0.48	0.44	0.35	0.26	0.45	0.30	0.18	0.24	0.23	0.23	0.28	0.49	0.40	0.40	0.39	0.35
Yb	2.81	2.84	2.80	2.79	2.19	1.65	2.78	1.85	1.13	1.47	1.44	1.37	1.69	3.21	2.63	2.46	2.55	2.14
Lu	0.4	0.4	0.4	0.4	0.3	0.2	0.3	0.2	0.1	0.2	0.2	0.2	0.2	0.47	0.38	0.3	0.3	0.3

	1	1	0	2	3	4	8	4	8	2	1	3	6			7	8	1
Hf	4.71	4.66	4.74	4.77	3.99	2.37	4.14	2.67	1.24	0.94	0.93	0.94	1.09	3.31	2.35	2.74	2.10	2.59
Ta	1.59	1.67	1.64	1.41	1.49	0.85	1.55	0.93	0.10	0.14	0.15	0.11	0.13	0.63	0.52	0.50	0.47	0.47
Pb	4.0	4.7	2.0	10.0	3.3	2.0	4.2	1.9	3.7	1.9	1.5	1.8	1.8	4.2	5.3	4.2	5.0	4.8
Th	3.88	3.83	3.74	4.33	3.09	1.85	3.59	2.13	0.81	0.70	0.65	0.68	0.91	2.60	2.00	2.04	1.94	6.30
U	0.97	0.96	0.98	1.00	0.78	0.41	0.78	0.51	0.17	0.15	0.14	0.15	0.18	0.68	0.50	0.61	0.48	1.15

Table 2 Sr-Nd isotopic compositions of the selected samples from the Yushu mafic rocks

Sample no.	$^{87}Rb/^{86}Sr$	$^{87}Sr/^{86}Sr$	±2σ	$^{147}Sm/^{144}Nd$	$^{143}Nd/^{144}Nd$	±2σ	t(Ma)	Isr	$\varepsilon_{Nd}(t)$
YS30-3	0.1360	0.706057	8	0.1352	0.512569	5	260	0.706	0.7
YS31-4	0.1245	0.706712	6	0.1391	0.512548	3	260	0.706	0.2
YS31-5	0.1283	0.707374	7	0.1325	0.512551	4	260	0.707	0.4
RN06-1	0.1343	0.709286	6	0.1348	0.512534	5	260	0.709	0.0
DC03-1	0.0646	0.707587	5	0.1446	0.512565	6	260	0.707	0.3
DC04-1	0.1754	0.707148	7	0.1372	0.512564	3	260	0.706	0.5
HX01-1	0.1205	0.712401	4	0.2176	0.51266	9	260	0.712	-0.3
HX02-1	0.1014	0.7096266	10	0.2179	0.5126748	14	260	0.709	0.0
HX03-1	0.1791	0.7106348	10	0.2153	0.5126564	11	260	0.710	-0.3
HX05-1				0.2465	0.51269	7	260		-0.6
PNG29-2				0.1942	0.512574	3	260		-1.2
PNQ29-1	0.3715	0.7126675	9	0.1784	0.5125446	5	260	0.711	-1.2
NQ15-3	0.2056	0.7087004	11	0.1859	0.5125682	8	260	0.708	-1.0
11MD01-2*		0.704283	4		0.512858	4			
11MD01-2*		0.704286	7		0.512866	3			

* Replicate analyses at the State Key Laboratory of Geological Processes and Mineral Resources (GPMR), China University of Geosciences (Wuhan).

Highlights

- An integrated study of the upper Permian Yushu mafic rocks in the central Tibetan Plateau was conducted to evaluate the interaction between the Emeishan mantle plume and the Paleo-Tethyan subduction system.
- The Group 1 rocks might be derived from a plume-related mantle source, whereas the Group 2 and Group 3 rocks originated from subduction-modified asthenospheric mantle and lithospheric mantle.
- A model involving plume-subduction interaction accounts for the geodynamics and generation of the late Permian mafic magmatism